AD_____

AWARD NUMBER: W81XWH-12-1-0348

TITLE: Activation of Myeloid-Derived Suppressor Cells in Bone Marrow

PRINCIPAL INVESTIGATOR: Serk In Park

RECIPIENT: The Vanderbilt University, Nashville TN 37240-0001

REPORT DATE: December 2013

TYPE OF REPORT: Final

PREPARED FOR: U.S. Army Medical Research and Materiel Command
Fort Detrick, Maryland 21702-5012

DISTRIBUTION STATEMENT: Approved for Public Release

REPORT DOCUMENTATION PAGE

Form Approved
OMB No. 0704-0188

1. REPORT DATE	2. REPORT TYPE	3. DATES COVERED
December 2013	Final	30September2012-29September2013

4. TITLE AND SUBTITLE
Activation of Myeloid-Derived Suppressor Cells in Bone Marrow

5a. CONTRACT NUMBER

5b. GRANT NUMBER
W81XWH-12-1-0348

5c. PROGRAM ELEMENT NUMBER

6. AUTHOR(S)
Serk In Park

email:serkin.park@vanderbilt.edu

5d. PROJECT NUMBER

5e. TASK NUMBER

5f. WORK UNIT NUMBER

7. PERFORMING ORGANIZATION NAME(S) AND ADDRESS(ES)
The Vanderbilt University, Nashville TN 37240-0001

8. PERFORMING ORGANIZATION REPORT NUMBER

9. SPONSORING / MONITORING AGENCY NAME(S) AND ADDRESS(ES)
U.S. Army Medical Research and Materiel Command
Fort Detrick, Maryland 21702-5012

10. SPONSOR/MONITOR'S ACRONYM(S)

11. SPONSOR/MONITOR'S REPORT NUMBER(S)

12. DISTRIBUTION / AVAILABILITY STATEMENT
Approved for Public Release; Distribution Unlimited

13. SUPPLEMENTARY NOTES

14. ABSTRACT
The overall goal of this research project was to investigate the mechanism of myeloid-derived suppressor cell (MDSC) activation within the bone marrow, in response to prostate cancer. The specific aims were designed to determine the effects of PTHrP-stimulated cytokine expression by osteoblasts on phosphorylation of Y418 Src family kinases in MDSs within the bone marrow, and to elucidate the effects of Src family kinases inhibition specifically in MDSCs on prostate tumor growth and angiogenesis. Experimental results from this study demonstrated that PTHrP drives an MDSC-mediated positive feedback loop to support prostate cancer growth. Furthermore, this study demonstrated that PTHrP increased tyrosine 418 residue phosphorylation levels in Src family kinases in MDSCs via osteoblast-derived IL-6 and VEGF-A, thereby upregulating MMP-9.

15. SUBJECT TERMS- none provided

16. SECURITY CLASSIFICATION OF:			17. LIMITATION OF ABSTRACT	18. NUMBER OF PAGES	19a. NAME OF RESPONSIBLE PERSON
a. REPORT	b. ABSTRACT	c. THIS PAGE			USAMRMC
U	U	U	UU	25	19b. TELEPHONE NUMBER *(include area code)*

Table of Contents

1. INTRODUCTION:

The major goal of this Exploration-Hypothesis Development Award was to determine how myeloid-derived suppressor cells (MDSCs) are activated in the bone marrow of prostate cancer hosts to promote tumor angiogenesis. MDSCs are bone marrow-derived cells in the tumor microenvironment, contributing to host immune surveillance and tumor progression. Beyond their critical functions, little is known about the regulation of MDSCs within their organ of origin (i.e. bone marrow) by distant primary tumor cells (1). This proposal examined whether parathyroid hormone-related peptide (PTHrP), an important bone-regulatory protein expressed by prostate cancer cells, mediates the potential crosstalk between prostate cancer and the bone marrow (2). As osteoblasts are the predominant cells responding to PTH/PTHrP, the specific aims of this proposal examined the effects of osteoblastic factors, including receptor activator of nuclear factor kappa B ligand (RANKL), interleukin (IL)-6, vascular endothelial growth factor (VEGF)-A and C-C chemokine ligand (CCL)-2, on activation of MDSCs within the bone marrow of prostate tumor hosts expressing varying levels of PTHrP. Furthermore, as a proposed mechanism of MDSC activation, phosphorylation of the Src family of non-receptor protein tyrosine kinases (SFKs) in MDSCs of PTHrP-expressing prostate tumor hosts was examined.

2. KEYWORDS:

Prostate cancer, metastasis, microenvironment, bone, Src family kinases, myeloid-derived suppressor cells, parathyroid hormone-related protein

3. OVERALL PROJECT SUMMARY:

The overall hypothesis of this study was that activating phosphorylation of Src family kinases by prostate cancer-stimulated osteoblasts confers angiogenic potential to myeloid-derived suppressor cells within the bone marrow. Two specific aims were designed: 1) to determine the effects of PTHrP-stimulated cytokine expression by osteoblasts on phosphorylation of Y^{418} Src family kinases in MDSCs within bone marrow, and 2) to elucidate the effects of Src family kinase specifically in MDSCs on prostate cancer growth and angiogenesis. We employed both *in vitro* and *in vivo* approaches.

The research results of this award over the course of 1-year support produced two recent publications in *Cancer Research* and *the Proceedings of the National Academy of Sciences of the U.S.A.* (*PNAS*). Therefore, detailed description of specific aspects of the research accomplishments is substituted with the papers in the appendix, and only briefly summarized in this final report.

As a first experimental approach, we examined whether phosphorylation of tyrosine 418 residue of Src family kinases (hereafter pY^{418} SFK) was increased in the $CD11b^{+}Gr1^{+}$ bone marrow cells in response to PTHrP-expressing prostate cancer. Flow cytometric analyses showed that pY^{418} SFK expression was significantly increased in the MDSCs isolated from the bone marrow of the mice carrying PTHrP-expressing prostate tumors, compared with the MDSCs isolated from non-PTHrP-expressing prostate tumors. This data suggest that alterations in the bone marrow via tumor-derived PTHrP contribute to activation of MDSCS in the bone marrow. In addition, this data support that tumor-derived PTHrP acts on bone via an endocrine manner. Further details of the results, including data figures, methodology, *etc*. are described in the Figures 1, 2 and 5 of the manuscript published in *Cancer Research* (3) (Appendix 1).

In addition, we observed that recombinant PTHrP treatment increased pY^{418} SFK expression in $CD11b^{+}Gr1^{+}$ MDSCs, suggesting the effects of the prostate tumor-induced pY^{418} SFK expression in MDSCs are mediated by PTHrP (refer to Figure 5 of the Appendix 1). An additional *in vivo* experiment was performed to further determine the kinetics of PTHrP-induced SFK phosphorylation. Briefly, PTHrP-releasing Alzet osmotic pumps were subcutaneously implanted in male mice, followed by flow cytometric analyses of phospho-Y418 SFK^{+} $CD11b^{+}Gr1^{+}$ bone marrow cells at 2, 12 and 36 hour time points. The 0-hour point (basal) was used as a control. Phospho-Y418 SFK expression was increased within 12 hours which was normalized after 36 hours (refer to the figure below).

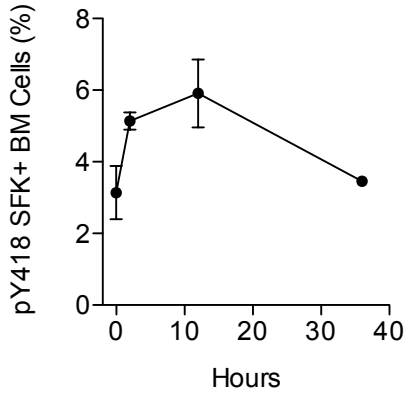

Subsequently, we compared the angiogenic potential between PTHrP-conditioned *vs.* control MDSCs *in vivo*. For this experiment, we isolated MDSCs from the bone marrow of the mice carrying PTHrP-expressing vs. control tumors (i.e. activated vs. control MDSCs). We then co-injected the MDSCs with prostate cancer cells in the subcutaneous space of male athymic mice. Upon necropsy, we performed immunohistochemical staining of prostate tumor tissue and quantification of mean vessel density between tumor tissues co-implanted with activated *vs.* control MDSCs. We found that prostate tumors co-implanted with activated MDSCs (i.e. MDSCs with higher pY^{418} SFK expression) resulted in increased mean vessel density, suggesting that pY^{418} SFK increase angiogenic potential of MDSCs.

We determined whether angiogenic potential of $CD11b^{+}Gr1^{+}$ MDSCs treated *ex vivo* with a SFK inhibitor or control buffer, followed by orthotopic co-implantation with PCa cells. To measure angiogenic potential of MDSCs, we compared the levels of MMP-9 (matrix metalloproteinases-9) because our data in Figures 1-5 of the manuscript published in *Cancer Research* (Appendix 1) showed that expression of *Mmp9* is the mechanism of MDSC-dependent tumor angiogenesis. We found that MDSCs treated with a SFK inhibitor (PP2) *ex vivo* had significantly reduced expression and activity of MMP-9, suggesting that suppression of SFK in MDSCs decrease the pro-angiogenic activities of MDSCs.

We administered anti-PTHrP neutralizing antibodies to the mice carrying PC-3 prostate tumors. We observed that anti-PTHrP neutralizing antibody suppressed MDSC functions, leading to decreased tumor growth and angiogenesis (as determined by immunohistochemistry and immunofluorescence staining in the Figure 7 of Appendix 1).

4. KEY RESEARCH ACCOMPLISHMENTS:

- Expression of pY^{418} SFK in $CD11b^{+}Gr1^{+}$ MDSCs was increased in the bone marrow of the murine hosts carrying PTHrP-expressing compared with MDSCs from the mice bearing non-PTHrP-expressing PCa.
- Recombinant PTHrP (1-34) increased pY^{418} SFK expression in $CD11b^{+}Gr1^{+}$ MDSCs from the bone marrow of the mice.
- Continuous release of PTHrP in the mice induced peak pY418 SFK expression at 12-hour time point.
- PTHrP-conditioned MDSCs had increased angiogenic potentials.
- *Ex vivo* treatment of PTHrP-conditioned MDSCs with a SFK inhibitor reduced angiogenic potentials.
- Anti-PTHrP neutralizing antibody decreased the pro-angiogenic function of MDSCs *in vivo*, leading to decreased tumor growth and angiogenesis.

5. CONCLUSION:

In conclusion, this study provided new evidence that distant prostate tumors stimulate the bone marrow to activate MDSCs in the tumor microenvironment. Prostate cancer-derived PTHrP circulates to potentiate $CD11b^{+}Gr1^{+}$ cells within the bone marrow via upregulation of IL-6 and VEGF-A in osteoblasts, contributing to tumor growth and angiogenesis. As a proposed mechanism of $CD11b^{+}Gr1^{+}$ cell potentiation, these data demonstrated that PTHrP increased activating phosphorylation of SFKs that subsequently increased *Mmp9* gene expression in $Cd11b^{+}Gr1^{+}$ cells, supporting that $CD11b^{+}Gr1^{+}$ cell-dependent tumor growth is, at least in part, mediated by MMP-9 expression and angiogenesis.

6. PUBLICATIONS, ABSTRACTS, AND PRESENTATIONS:

a. List all manuscripts submitted for publication during the period covered by this report resulting from this project:

(1) Lay Press: None

(2) Peer-Reviewed Scientific Journals:

Park SI, Lee C, Sadler WD, Koh AJ, Jones J, Seo JW, Soki FN, Cho SW, Daignault SD, McCauley LK. Parathyroid hormone-related protein drives a CD11b+Gr1+ cell-mediated positive feedback loop to support prostate cancer growth. Cancer Res. 2013 Nov 15. 73(22):6574-83. PMCID: PMC3838921

Cho SW, Soki FN, Koh AJ, Eber M, Entezami P, **Park SI**, van Rooijen N, McCauley LK. Osteal macrophages support physiologic skeletal remodeling and anabolic actions of parathyroid hormone in bone. Proceedings of the National Academy of Sciences of the U.S.A. 2014 Jan 28; 111(4):1545-50. PMCID: in process

(3) Invited Articles: None

(4) Abstracts: None

b. List presentations made during the last year:

1) **Park SI**, Koh AJ, Soki FN, McCauley LK. Parathyroid hormone-related protein (PTHrP) potentiates myeloid-derived suppressor cells (MDSCs) within the bone marrow via osteoblast-derived interleukin (IL)-6 and vascular endothelial growth factor (VEGF)-A. American Society of Bone and Mineral Resaerch 2012 Annual Meeting, Oral and plenary poster (Abstract No. FR0440)
2) **Park SI**, Koh AJ, Soki FN, McCauley LK. Parathyroid hormone-related protein (PTHrP) potentiates myeloid-derived suppressor cells (MDSCs) within the bone marrow via osteoblast-derived interleukin (IL)-6 and vascular endothelial growth factor (VEGF)-A. The International Bone and Mineral Society's 12th International Conference on Cancer-Induced Bone Disease, Short-talk presentation

7. INVENTIONS, PATENTS AND LICENSES: None

8. REPORTABLE OUTCOMES:

1. Young Investigator Award, the American Society of Bone and Mineral Research, 2012
    a. This prestigious award was given in recognition of the scientific merit of the presentation (referenced in the above 6-b)-1 section).
2. Two peer-reviewed scientific publications
    a. **Park SI**, Lee C, Sadler WD, Koh AJ, Jones J, Seo JW, Soki FN, Cho SW, Daignault SD, McCauley LK. Parathyroid hormone-related protein drives a

CD11b+Gr1+ cell-mediated positive feedback loop to support prostate cancer growth. Cancer Res. 2013 Nov 15. 73(22):6574-83. PMCID: PMC3838921

b. Cho SW, Soki FN, Koh AJ, Eber M, Entezami P, **Park SI**, van Rooijen N, McCauley LK. Osteal macrophages support physiologic skeletal remodeling and anabolic actions of parathyroid hormone in bone. Proceedings of the National Academy of Sciences of the U.S.A. 2014 Jan 28; 111(4):1545-50. PMCID: in process

9. OTHER ACHIEVEMENTS:

Based on the results from this Exploration-Hypothesis Development Award, three research proposals were submitted.

1) FY 2012 Department of Defense Prostate Cancer Research Program Idea Development Award
2) American Cancer Society Research Scholar Program
3) National Cancer Institute R21 Grant

10. REFERENCES:

1. Park SI, Soki FN, McCauley LK. Roles of bone marrow cells in skeletal metastases: no longer bystanders. Cancer Microenviron. 2011 Dec;4(3):237–46.

2. Park SI, McCauley LK. Nuclear localization of parathyroid hormone-related peptide confers resistance to anoikis in prostate cancer cells. Endocr Relat Cancer. 2012;19(3):243–54.

3. Park SI, Lee C, Sadler WD, Koh AJ, Jones J, Seo JW, et al. Parathyroid Hormone-Related Protein Drives a CD11b+Gr1+ Cell-Mediated Positive Feedback Loop to Support Prostate Cancer Growth. Cancer Res. 2013 Nov 14;73(22):6574–83.

11. APPENDICES:

Appendix 1: Park SI, *et al.* Parathyroid hormone-related protein drives a CD11b+Gr1+ cell-mediated positive feedback loop to support prostate cancer growth. Cancer Res. 2013 Nov 15. 73(22):6574-83. PMCID: PMC3838921

Appendix 2: Cho SW, *et al*. Osteal macrophages support physiologic skeletal remodeling and anabolic actions of parathyroid hormone in bone. Proceedings of the National Academy of Sciences of the U.S.A. 2014 Jan 28; 111(4):1545-50. PMCID: in process

Published OnlineFirst September 26, 2013; DOI: 10.1158/0008-5472.CAN-12-4692

Appendix 1

Cancer Research

Parathyroid Hormone–Related Protein Drives a CD11b^{+}Gr1^{+} Cell–Mediated Positive Feedback Loop to Support Prostate Cancer Growth

Serk In Park, Changki Lee, W. David Sadler, et al.

Cancer Res 2013;73:6574-6583. Published OnlineFirst September 26, 2013.

Published OnlineFirst September 26, 2013; DOI: 10.1158/0008-5472.CAN-12-4692

Microenvironment and Immunology

Cancer Research

Parathyroid Hormone–Related Protein Drives a CD11b$^+$Gr1$^+$ Cell–Mediated Positive Feedback Loop to Support Prostate Cancer Growth

Serk In Park[1,2,3,4,5], Changki Lee[1,3], W. David Sadler[5], Amy J. Koh[5], Jacqueline Jones[5], Jung Won Seo[1], Fabiana N. Soki[5], Sun Wook Cho[5], Stephanie D. Daignault[6], and Laurie K. McCauley[5,7]

Abstract

In the tumor microenvironment, CD11b$^+$Gr1$^+$ bone marrow–derived cells are a predominant source of protumorigenic factors such as matrix metalloproteinases (MMP), but how distal tumors regulate these cells in the bone marrow is unclear. Here we addressed the hypothesis that the parathyroid hormone–related protein (PTHrP) potentiates CD11b$^+$Gr1$^+$ cells in the bone marrow of prostate tumor hosts. In two xenograft models of prostate cancer, levels of tumor-derived PTHrP correlated with CD11b$^+$Gr1$^+$ cell recruitment and microvessel density in the tumor tissue, with evidence for mediation of CD11b$^+$Gr1$^+$ cell–derived MMP-9 but not tumor-derived VEGF-A. CD11b$^+$Gr1$^+$ cells isolated from mice with PTHrP-overexpressing tumors exhibited relatively increased proangiogenic potential, suggesting that prostate tumor–derived PTHrP potentiates this activity of CD11b$^+$Gr1$^+$ cells. Administration of neutralizing PTHrP monoclonal antibody reduced CD11b$^+$Gr1$^+$ cells and MMP-9 in the tumors. Mechanistic investigations *in vivo* revealed that PTHrP elevated Y418 phosphorylation levels in Src family kinases in CD11b$^+$Gr1$^+$ cells via osteoblast-derived interleukin-6 and VEGF-A, thereby upregulating MMP-9. Taken together, our results showed that prostate cancer–derived PTHrP acts in the bone marrow to potentiate CD11b$^+$Gr1$^+$ cells, which are recruited to tumor tissue where they contribute to tumor angiogenesis and growth. *Cancer Res; 73(22); 6574–83. ©2013 AACR.*

Introduction

The tumor microenvironment provides primary tumor cells to mix with multiple types of stroma such as endothelium, fibroblasts, and immune cells (1). Such heterogeneity of cell populations presents a major impediment for developing a cure for cancer. Increasing evidence supports that stromal cells in the tumor microenvironment not only occupy a significant fraction of the tumor bulk, but also play critical roles in proliferation, invasion, and/or metastasis of tumor cells (2). In this regard, bone is an essential partner for tumor progression, because bone marrow serves as the supplying organ for numerous critical cells in the tumor microenvironment (3, 4). However, it is unclear how tumor cells co-opt the bone and/or bone marrow to facilitate a favorable tumor microenvironment.

Authors' Affiliations: Departments of [1]Medicine and [2]Cancer Biology; [3]Center for Bone Biology; [4]Vanderbilt-Ingram Cancer Center, Vanderbilt University School of Medicine, Nashville, Tennessee; [5]Department of Periodontics and Oral Medicine, University of Michigan School of Dentistry; [6]Comprehensive Cancer Center Biostatistics Core; and [7]Department of Pathology, University of Michigan Medical School, Ann Arbor, Michigan

Note: Supplementary data for this article are available at Cancer Research Online (http://cancerres.aacrjournals.org/).

Corresponding Author: Laurie K. McCauley, Department of Periodontics and Oral Medicine, University of Michigan School of Dentistry, 1011 N. University Avenue, Ann Arbor, MI 48109. Phone: 734-647-3206; Fax: 734-763-5503; E-mail: mccauley@umich.edu

doi: 10.1158/0008-5472.CAN-12-4692

Among the bone marrow–derived cells, CD11b$^+$Gr1$^+$ cells [commonly referred to as myeloid-derived suppressor cells (MDSC)] correlate with tumor progression (5). MDSCs were originally investigated for their roles in evasion of host immune surveillance, especially via suppression of T-cell–dependent antitumoral immunity by production of arginase, reactive oxygen species, and inducible nitric oxide synthase (6). Subsequent studies demonstrated that MDSCs are increased in tumor-bearing mice and cancer patients, and infiltrate primary tumor tissue to promote angiogenesis by secreting matrix metalloproteinases (MMP), and also by direct incorporation into tumor endothelium (7, 8). More recently, MDSCs have been shown to play key roles in recovery after radiation therapy (9, 10) and antiangiogenic therapy (11).

In parallel, multiple mechanisms have been proposed to explain the increased recruitment of MDSCs in tumor tissue. Yang and colleagues demonstrated that CXC chemokine ligand (CXCL)-5/CXC receptor (CXCR)-2 and stromal-derived factor-1/CXCR-4 axes recruit circulating MDSCs to tumor tissue (12). More recently, expression of a single integrin ($\alpha4\beta1$) promotes MDSC invasion into tumors via activation of phosphatidylinositol 3-kinase (PI3K; ref. 13). However, despite such clear evidence supporting the tumorigenic functions of MDSCs and also the potential mechanisms of recruitment to the tumor tissue, MDSCs are poorly understood about their regulation in the supplying organ (i.e., bone marrow) of the tumor host, and also their potential crosstalk with distant primary tumor cells.

Published OnlineFirst September 26, 2013; DOI: 10.1158/0008-5472.CAN-12-4692

This study was designed to elucidate how CD11b$^+$Gr1$^+$ cells are regulated in the bone marrow of prostate tumor hosts, contributing to tumor growth and angiogenesis. Prostate cancer provides a unique perspective on this process because of its devastating mortality and morbidity associated with its preferential metastasis to the skeleton (14). Accordingly, prostate cancer cells secrete numerous important bone-modulating cytokines, leading to osteoblastic/osteolytic reactions that facilitate growth factor and cytokine release from bone cells and matrix (15). In particular, parathyroid hormone–related protein (PTHrP) is expressed by prostate cancer cells, and stimulates osteoblasts in an endocrine manner to secrete factors such as receptor activator of NF-κB ligand (RANKL), interleukin (IL)-6, C-C chemokine ligand (CCL)-2, and VEGF-A within the bone microenvironment (16–18). Subsequently, PTHrP-induced cytokines have the ability to trigger cascades of unfavorable events (e.g., signaling pathways leading to potentiation of CD11b$^+$Gr1$^+$ bone marrow cells) within the bone marrow, contributing to tumor progression. Overall, the central hypothesis of this study was prostate cancer–derived PTHrP potentiates CD11b$^+$Gr1$^+$ cells within the bone marrow, contributing to angiogenesis and tumor growth.

Materials and Methods

Cells

Two luciferase-labeled PC-3 clones expressing high and low levels of PTHrP were selected from previously established stable-shRNA clones targeting *PTHLH* (19), designating PTHrP^{Hi} and PTHrP^{Lo}, respectively. Ace-1 canine prostate carcinoma cells, expressing undetectable basal levels of PTHrP, were stably transfected with a pcDNA3.1 vector expressing full-length mouse/rat PTHrP (17). An empty-vector transfectant was used as a control. Expression of PTHrP was confirmed from the culture supernatant using an immunoradiometric assay kit (Diagnostic Laboratories). PC-3 clones were regularly authenticated and matched short tandem repeat DNA profiles of the original PC-3 cell line (last tested on August 28, 2012).

Mice and *in vivo* tumors

All mouse experiments were approved by the Institutional Animal Care and Use Committees of the University of Michigan and Vanderbilt University. For *in vivo* tumors, 1×10^6 prostate tumor cells were suspended in 100 μL Hank's balanced salt solution and 1:1 mixed with growth factor–reduced Matrigel (BD Biosciences), followed by subcutaneous injection into male athymic mice (Harlan Laboratories) as previously described (20, 21). Mice were regularly monitored for morbidity or tumor growth, and tumor size was calculated using an equation: Volume $= {}^1/_2 \times a \times b^2$, where a is the long diameter and b is the short diameter measured with a caliper (22). Anti-human PTHrP 1 to 33 monoclonal antibodies (hybridoma 158) were produced and generously gifted by Dr. R. Kremer (McGill University, Montreal, Quebec, Canada; ref. 18). Mice were treated with anti-PTHrP monoclonal antibody (200 μL) or mouse immunoglobulin G (IgG; Sigma-Aldrich) by every other day intraperitoneal injection for the first 3 weeks, followed by daily injection for 1 week before euthanasia.

Flow cytometry

For analyses of CD11b$^+$Gr1$^+$ cells in the tumor tissue, tumors were mechanically dissociated, followed by digestion in complete RPMI-1640 media supplemented with type I collagenase (5 mg/mL; Sigma-Aldrich). Viable cells were counted and resuspended in fluorescence-activated cell sorting buffer containing combinations of antibodies including FITC-conjugated anti-mouse CD11b, PE-conjugated anti-mouse Gr1, or isotype controls. For analyses or sorting CD11b$^+$Gr1$^+$ cells from the bone marrow, the femoral bone marrow was flushed and dissociated, followed by antibody staining and flow cytometry (23). For analyses of phospho-Y^{418} Src family kinase (SFK), the bone marrow cells were fixed, permeabilized, stained, and analyzed according to the BD PhosFlow Cell Signaling protocols. All materials were from BD Biosciences.

Immunohistochemistry

Tumors were surgically removed and bisected, a portion fixed in formalin and a portion snap-frozen. Murine endothelial cell–specific CD31/PECAM immunostaining (clone MEC13.3; BD Biosciences) was performed according to a previously described method (24). Rat anti-mouse CD11b (clone M1/70; BD Biosciences) and anti-mouse Ly-6G (clone RB6-8C5; eBioscience) were fluorescently labeled and used to detect CD11b$^+$Gr1$^+$ cells in the tumor tissue. Three to five randomly selected microscopic images per sample were obtained, and positively stained cells were counted using ImageJ software.

Quantitative PCR

mRNA samples were prepared from the bone marrow or tumor tissues using TRIzol reagent (Invitrogen), followed by reverse transcription-quantitative PCR (25). All quantitative PCR probes and reagents were from Applied Biosystems.

Statistical analyses

All *in vivo* data sets were tested for normality by Shapiro–Wilk test. Statistical analyses were performed by GraphPad Prism software. Student t test or Mann–Whitney U test were used to compare 2 groups and all statistical tests were 2-sided.

Results

Reduction of PTHrP in PC-3 prostate tumors decreased CD11b$^+$Gr1$^+$ bone marrow cell recruitment and angiogenesis

As a first approach to investigate the role of PTHrP in the potential crosstalk between tumor and the bone marrow, the *PTHLH* gene (encoding PTHrP) was targeted via lentiviral shRNA vectors in PC-3, human prostate cancer cells (19). Two clones expressing high and low levels of PTHrP (961.8 ± 12.8 vs. 457.8 ± 4.1 pg mL^{-1} 1×10^6 cells^{-1} 48 h^{-1}; measured in the culture supernatant by immunoradiometric assays) were selected and designated PTHrP^{Hi} and PTHrP^{Lo}, respectively. PTHrP is well known to regulate tumor growth via autocrine, intracrine, and paracrine manners (17–19, 26, 27), hence alterations in the host response (e.g., recruitment of host-derived cells) could simply be secondary to the differences in

Published OnlineFirst September 26, 2013; DOI: 10.1158/0008-5472.CAN-12-4692

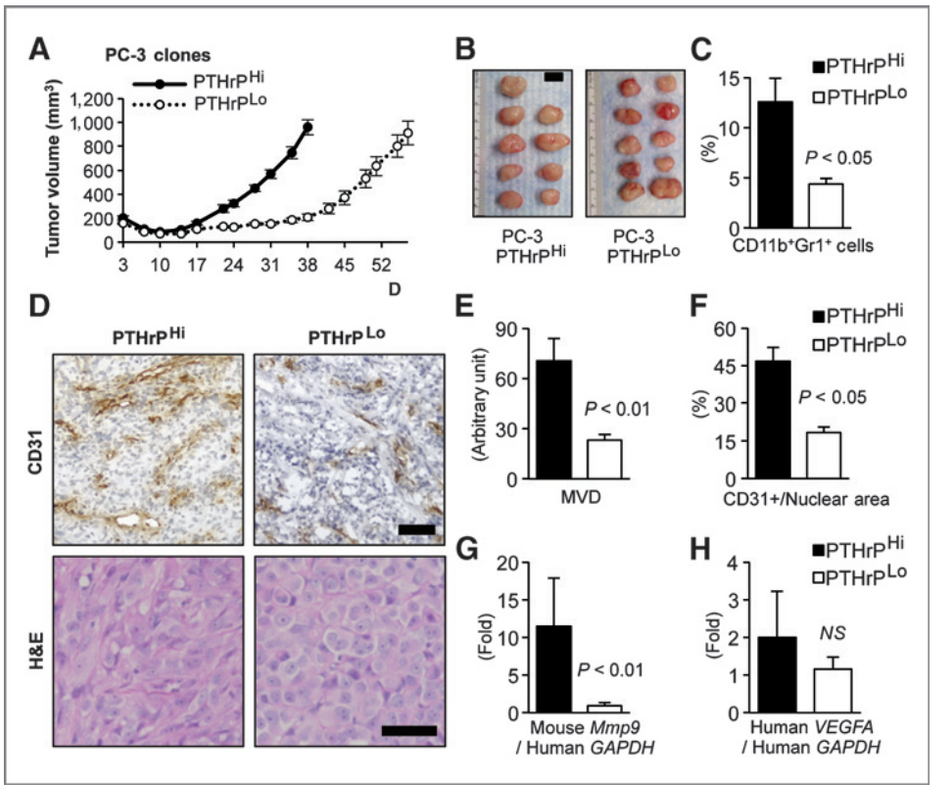

Figure 1. Reduction of PTHrP in PC-3 prostate tumors decreased $CD11b^+Gr1^+$ MDSC recruitment and angiogenesis. A, tumor growth curve of PC-3 clones expressing high or low levels of PTHrP ($n = 9$ for $PTHrP^{Hi}$ and $n = 10$ for $PTHrP^{Lo}$). $PTHrP^{Lo}$ tumors were grown for a longer period (57 days) to reach a similar mean tumor volume as $PTHrP^{Hi}$ tumors (38 days). B, $PTHrP^{Hi}$ and $PTHrP^{Lo}$ tumors were surgically dissected on the same day and photographed. Mean tumor volume between the 2 groups was not significantly different ($P = 0.68$, Student t test). Scale bar, 1 cm. C, percentages of $CD11b^+Gr1^+$ double-positive cells in the tumor tissues were analyzed by flow cytometry. D, tumor tissues were sectioned for H&E and murine CD31/PECAM immunohistochemical staining. Original magnification, ×20. Scale bars, 50 μm. E and F, microscopic images were analyzed for tumor mean vessel density (MVD) or $CD31^+$ vascular area with normalization to total nuclear area. G and H, host-derived (i.e., murine) *Mmp9* and tumor-derived (i.e., human) *VEGFA* mRNA levels were measured by quantitative RT-PCR using species-specific probes ($n = 9$–10 per group). All P values are from Student t test. *NS*, not significant. Data in all graphs are mean ± SEM.

the tumor size, not in PTHrP expression levels. Therefore, $PTHrP^{Lo}$ tumors were grown for a longer period until they reached a similar mean tumor volume as $PTHrP^{Hi}$ tumors to circumvent the direct tumor-size effects in the subsequent analyses (Fig. 1A and B). Flow cytometric analyses of the tumor tissues revealed that $PTHrP^{Lo}$ tumors had significantly reduced percentages of $CD11b^+Gr1^+$ cells in the tumor tissue compared with $PTHrP^{Hi}$ tumors (Fig. 1C). Immunohistological analyses showed PTHrP levels correlated with mean vessel density and vessel area of PC-3 tumors (Fig. 1D–F). A well-characterized mechanism of MDSC-dependent tumor angiogenesis is through the expression of MMP-9 (7, 28). Accordingly, tumor tissues were analyzed for expression of host-derived MMP-9 expression as well as tumor-derived VEGF-A (Fig. 1G and H) using species-specific PCR probes. $PTHrP^{Lo}$ tumors had significantly reduced host-derived (i.e., murine) *Mmp9* expression, whereas no significant reduction in the tumor-derived (i.e., human) *VEGFA* was observed. Collectively, reduction of PTHrP in PC-3 prostate tumors decreased $CD11b^+Gr1^+$ cell recruitment and tumor angiogenesis, in association with reduced expression of host MMP-9 but not of tumor VEGF-A.

Ectopic PTHrP increased the recruitment of $CD11b^+Gr1^+$ cells in prostate tumor tissue

An additional prostate tumor model was utilized to establish the causal relationship between PTHrP and $CD11b^+Gr1^+$ cells. Ace-1 prostate cancer cells produce predominantly osteoblastic lesions *in vivo*, a phenotype that recapitulates human prostate cancer more realistically than the majority of currently available prostate cancer cell lines (17, 29). Ace-1 cells, expressing undetectable basal levels of PTHrP, were stably transfected with PTHrP overexpression (designated PTHrP OE) or empty control (designated pcDNA) vectors. In the same approach as the PC-3 tumor model (i.e., growth in differential periods), 2 groups of similarly sized tumors, PTHrP OE and pcDNA control, were produced. To directly examine the effects of systemic PTHrP on $CD11b^+Gr1^+$ cell recruitment, one group of mice carrying pcDNA control tumors was treated with recombinant PTHrP (amino acids 1–34, a ligand-binding fragment) for 7 days before harvest (Fig. 2A and Supplementary Fig. S1). Both PTHrP OE and recombinant PTHrP-treated groups had significantly increased $CD11b^+Gr1^+$ cells in the tumor tissue compared with pcDNA control tumors (Fig. 2B). Although mice burdened with PTHrP OE tumors had

Published OnlineFirst September 26, 2013; DOI: 10.1158/0008-5472.CAN-12-4692

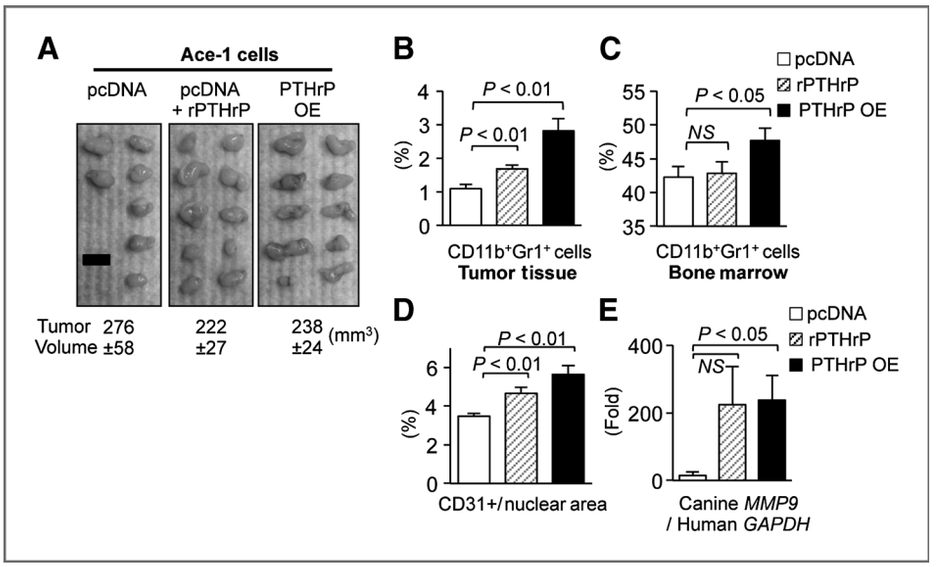

Figure 2. Ectopic PTHrP increased CD11b$^+$Gr1$^+$ cells in prostate tumors and in the bone marrow. Ace-1 prostate cancer cells, expressing undetectable basal levels of PTHrP, were engineered to overexpress PTHrP (PTHrP OE) with a vector-alone transfectant control (pcDNA). Cells were implanted subcutaneously in male athymic mice. A, PTHrP OE ($n = 10$; right) were grown for a shorter period (17 days) to produce similarly sized tumors as pcDNA control tumors ($n = 7$; grown for 32 days; left). In addition, one group of mice carrying pcDNA tumors ($n = 10$; middle) was administered recombinant PTHrP (1–34) once daily for 7 days before euthanasia (designated rPTHrP). Mean tumor volume ± SEM (mm^3) for each group is indicated. No statistical significance in tumor volume ($P > 0.05$ by Student *t* test) in any pair of groups. Scale bar, 1 cm. B and C, percentages of CD11b$^+$Gr1$^+$ cells in the tumor tissues or in the bone marrow were analyzed by flow cytometry. D, tumor tissues were analyzed for quantification of CD31$^+$ vessel area with normalization to total nuclear area ($n = 7$–10 per group). E, tumor-derived (i.e., canine) *MMP9* mRNA levels were measured ($n = 7$–10 per group). All *P* values are from Student *t* test. *NS*, not significant. Data in all graphs are mean ± SEM.

significantly increased percentages of CD11b$^+$Gr1$^+$ cells in the bone marrow (Fig. 2C), recombinant PTHrP treatment failed to show such an increase in the bone marrow. This may be explained by either the different modes of PTHrP administration (i.e., intermittent injection *vs.* continuous expression) or the reduced duration (7 days) of PTHrP treatment compared with tumor burden (21 days). Immunohistochemical analyses of tumor tissue showed that both PTHrP OE and recombinant PTHrP tumors had significantly increased evidence of angiogenesis (Fig. 2D and Supplementary Fig. S1B). In addition, host-derived *Mmp9* expression was significantly increased in PTHrP OE tumor tissue (Fig. 2E), suggesting contribution of the CD11b$^+$Gr1$^+$ cell recruitment, at least in part, to angiogenesis. Collectively, data in Figs. 1 and 2 suggest that prostate cancer-derived PTHrP is a crucial regulator of CD11b$^+$Gr1$^+$ cells.

CD11b$^+$Gr1$^+$ cells promoted tumor growth *in vivo*

The protumorigenic functions of CD11b$^+$Gr1$^+$ cells are relatively well characterized using multiple tumor models (5, 7, 30, 31). To more rigorously examine the effects of CD11b$^+$Gr1$^+$ cells on tumor growth in the prostate tumor model, 2 fractions of bone marrow cells, that is CD11b/Gr1-double positive or negative cells, were isolated and coimplanted with parental Ace-1 tumor cells *in vivo* (Fig. 3A). Increasing numbers of CD11b$^+$Gr1$^+$ cells mixed with tumor cells correspondingly increased the tumor size within 15 days (Fig. 3B and C). More importantly, Ace-1 tumor coimplanted with 0.5×10^6 CD11b$^+$Gr1$^+$ cells grew significantly larger than tumors coimplanted with the same number of CD11b$^-$Gr1$^-$ cells, suggesting that altered tumor size in Figs. 1 and 2 were secondary to the altered recruitment of CD11b$^+$Gr1$^+$ cells in the tumor tissue.

Tumor-derived PTHrP confers increased angiogenic potential to CD11b$^+$Gr1$^+$ cells

To examine whether tumor-derived PTHrP regulates CD11b$^+$Gr1$^+$ cells within the bone marrow of tumor hosts, CD11b$^+$Gr1$^+$ bone marrow cells were isolated from 2 groups of mice bearing either PTHrP-overexpressing or pcDNA control tumors for 3 weeks, resulting in 2 fractions of CD11b$^+$Gr1$^+$ cells (i.e., PTHrP-activated vs. control). Parental Ace-1 tumor cells were mixed with the isolated CD11b$^+$Gr1$^+$ cells and xenografted into male athymic mice (Fig. 4A). Tumors coimplanted with PTHrP-activated CD11b$^+$Gr1$^+$ cells were significantly larger than the tumors with control CD11b$^+$Gr1$^+$ cells (Fig. 4B), potentially because increased MMP-9 and angiogenesis as determined by immunohistochemistry (Fig. 4C and D and Supplementary Fig. S2).

PTHrP increased expression of phospho-[Y^{418}] Src family kinases in CD11b$^+$Gr1$^+$ cells

The molecular mechanism for the observed PTHrP-dependent CD11b$^+$Gr1$^+$ cell potentiation was subsequently investigated. Recently, Liang and colleagues demonstrated that dasatinib, an SFK inhibitor, suppressed prostate tumor growth as well as the numbers of CD11b$^+$ myeloid cells in tumor tissues (32). Accordingly, the effects of PTHrP administration

Published OnlineFirst September 26, 2013; DOI: 10.1158/0008-5472.CAN-12-4692

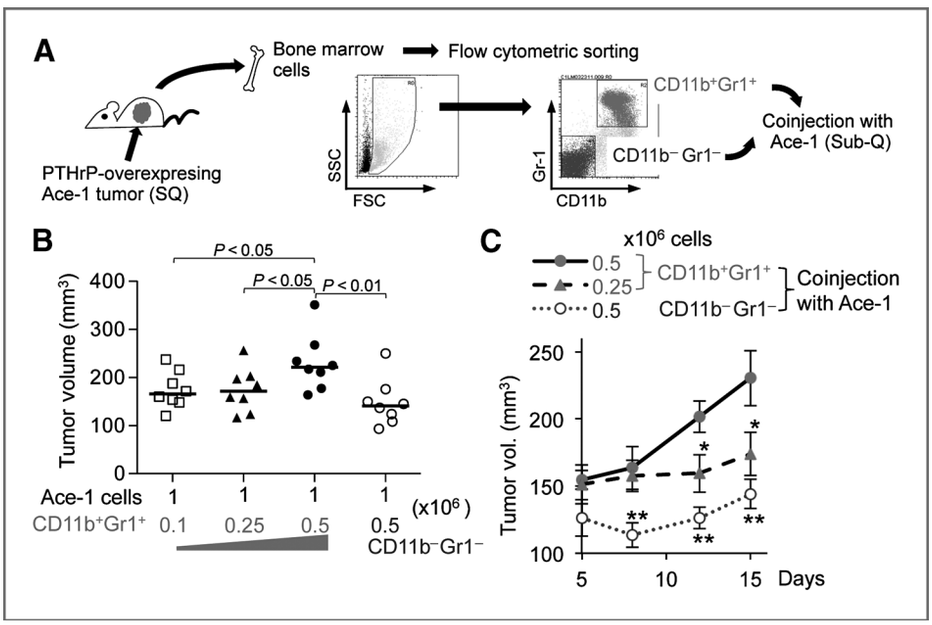

Figure 3. $CD11b^+Gr1^+$ cells promoted tumor growth *in vivo*. A, schematic representation of the experiment. Male athymic mice were implanted with PTHrP-overexpressing Ace-1 tumors for 21 days before harvesting femoral bone marrow cells. Flow cytometric sorting resulted in 2 fractions of CD11b/Gr1 double positive or double negative cells, followed by their coinjection with parental Ace-1 cells subcutaneously in male athymic mice ($n = 8$ per group). B, individual tumor size was measured 15 days after xenograft and plotted on a graph. Dots, individual tumor volumes (mm^3). Horizontal lines, medians. *P* values are from Student *t* test. C, tumor growth curve was plotted to compare growth kinetics. Data are mean ± SEM. *, $P < 0.05$ and **, $P < 0.01$, Student *t* test.

on SFK in $CD11b^+Gr1^+$ cells were investigated. A single administration of PTHrP (1–34) to male athymic mice significantly increased the activating phosphorylation of Tyr-418 residue of SFK in $CD11b^+Gr1^+$ cells (Fig. 5A). As SFK activation requires intramolecular conformational changes and interaction with activated receptor kinases via the SH-2 domain, phosphorylation of [Y^{418}] in the SH-2 domain indicates the status of full activation. However, because $CD11b^+Gr1^+$ cells do not express receptors for PTHrP (as determined by quantitative reverse transcription (RT)-PCR for *Pthr1*; Supplementary Fig. S3), phosphorylation of [Y^{418}] SFK was reasoned to be indirect through cytokines from osteoblasts, the predominant cells expressing the PTH/PTHrP receptor (PTH1R) in the bone marrow. Potential candidate cytokines from PTHrP-stimulated osteoblasts included IL-6, VEGF-A, C-C chemokine ligand (CCL)-2, and RANKL (16, 33–35). Therefore, $CD11b^+Gr1^+$ cells were isolated from femoral bone marrow and treated with these osteoblastic cytokines. Although all 4 cytokines (IL-6, VEGF-A, CCL-2, and RANKL) have been shown to upregulate SFKs (36–38), only IL-6 and VEGF-A increased the expression of phospho-[Y^{418}] SFK in MDSCs (Fig. 5B).

Phospho-[Y^{418}] SFK by osteoblastic VEGF-A and IL-6 increased MMP-9 expression in $CD11b^+Gr1^+$ cells

To further investigate the functional significance of phospho-[Y^{418}] SFKs in MDSCs, several published markers of

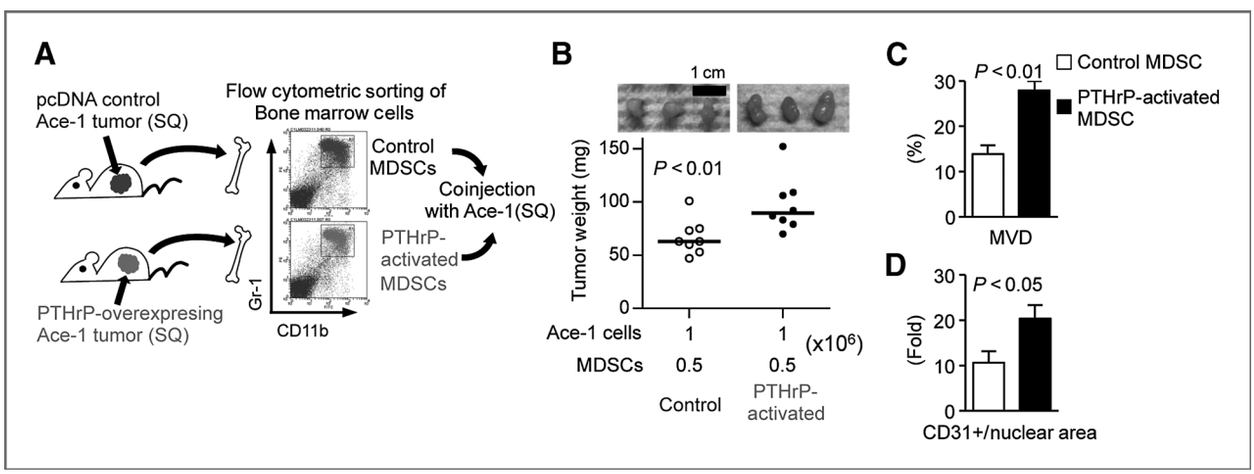

Figure 4. PTHrP promoted tumorigenic function of $CD11b^+Gr1^+$ bone marrow cells. A, schematic representation of the experiment. Two groups of male athymic mice ($n = 3$ per group) were implanted with PTHrP-overexpressing or control tumors for 21 days before flow cytometric sorting of $CD11b^+Gr1^+$ bone marrow cells. Subsequently, parental Ace-1 prostate tumor cells were coinjected with the primed $CD11b^+Gr1^+$ cells into male athymic mice ($n = 8$ per group). B, individual tumor weight was measured and plotted, and photographs of 3 representative tumors are shown. Dots, individual tumor weight (mg). Horizontal lines, median ($n = 8$ per group). C and D, tumor tissues were analyzed for quantification of $CD31^+$ mean vessel density or vessel area with normalization to total nuclear area. Data are mean ± SEM. All *P* values are from Student *t* test.

Published OnlineFirst September 26, 2013; DOI: 10.1158/0008-5472.CAN-12-4692

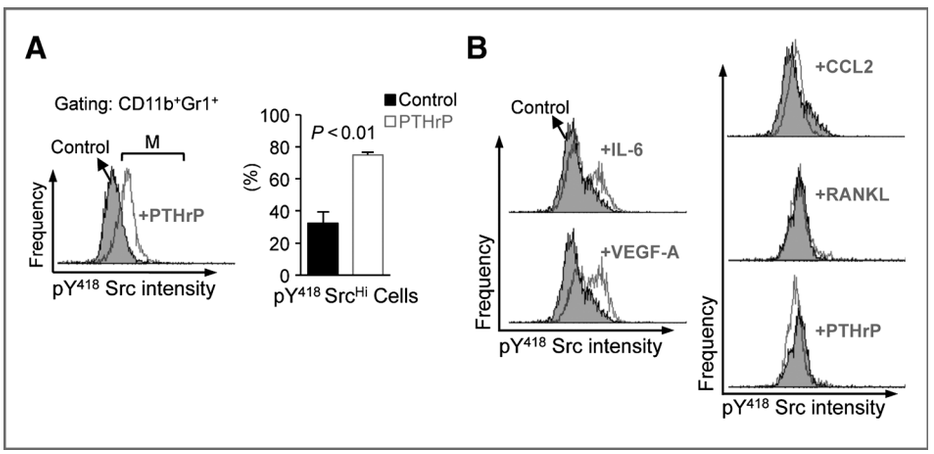

Figure 5. PTHrP phosphorylated [Y^{418}] Src family kinases in CD11b$^+$Gr1$^+$ cells. A, male athymic mice ($n = 3$ per group) were stimulated with a single administration of PTHrP (1–34) or saline control, 8 hours before sacrifice and flow cytometric analyses of phospho-[Y^{418}] Src family kinase expression levels in CD11b$^+$Gr1$^+$ bone marrow cells. Representative histograms from the control group (shaded) and the PTHrP-stimulated group (open) were overlapped to show the intensity of phospho-[Y^{418}] Src expression. CD11b$^+$Gr1$^+$ cells expressing high levels of phospho-[Y^{418}] Src family kinases [indicated by a bracket (M)] were quantified and plotted. Data are mean ± SEM. $P < 0.01$, Student t test. B, CD11b/Gr1 double positive cells were sorted from the femoral bone marrow of male athymic mice, followed by treatment with saline, IL-6, VEGF-A, CCL-2, RANKL, or PTHrP (all 100 ng/mL for 0.5×10^6 cells) for 1 hour at 37°C ($n = 3$ per group). Representative histograms (open) were overlapped onto unstimulated controls (shaded) to show the intensity of staining.

CD11b$^+$Gr1$^+$ cell activation were examined in combination with PTHrP-dependent osteoblastic cytokines and an SFK selective inhibitor, PP2 (5, 13, 28). Only VEGF-A and IL-6 increased *Mmp9* gene expression, whereas *Cxcr2*, *Cxcr4*, or *Itgb1* expression remained unaffected in CD11b$^+$Gr1$^+$ cells, and this increase was reversed by PP2 treatment (Fig. 6A–D).

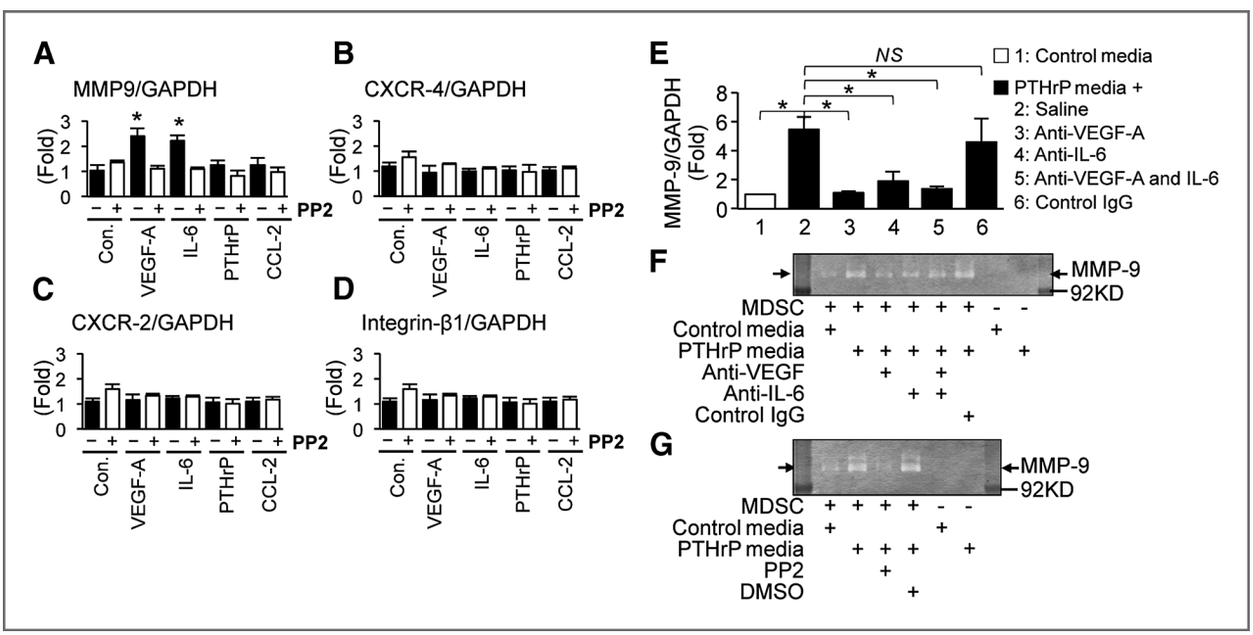

Figure 6. Phosphorylation of Src family kinases by osteoblastic VEGF-A and IL-6 increased MMP-9 expression in CD11b$^+$Gr1$^+$ cells. A–D, CD11b$^+$Gr1$^+$ cells were sorted from the femoral bone marrow of male athymic mice via flow cytometry, followed by treatment with saline (control), VEGF-A, IL-6, PTHrP, or CCL-2 (100 ng/mL for 0.5×10^6 cells) in combination with PP2 (an SFK inhibitor; 100 nmol/L) or dimethyl sulfoxide (DMSO) control for 1 hour at 37°C ($n = 3$ per group). mRNA levels of *Mmp9*, *Cxcr4*, *Cxcr2*, and *Itgb1* were determined via quantitative RT-PCR. Data are mean ± SEM. *, $P < 0.01$ compared with the DMSO control group. No other combination had statistical significance ($P > 0.05$, Student t test). E–G, conditioned media were collected from primary calvarial osteoblasts stimulated with saline (control) or PTHrP (1–34). Femoral bone marrow CD11b$^+$Gr1$^+$ cells were treated with the control or PTHrP-conditioned media in combination with neutralizing antibodies against VEGF-A and/or IL-6, followed by quantitative PCR (E) for *Mmp9* gene expression ($n = 3$ per group) or zymography (F). Data are mean ± SEM. *, $P < 0.05$; *NS*, not significant by Student t test. G, CD11b$^+$Gr1$^+$ cells were treated with control or PTHrP-conditioned media in combination with PP2 or DMSO control, followed by zymography.

Published OnlineFirst September 26, 2013; DOI: 10.1158/0008-5472.CAN-12-4692

Furthermore, to confirm the requirement of osteoblasts in PTHrP-dependent potentiation of $CD11b^+Gr1^+$ cells, primary osteoblasts were established from murine calvaria and treated with PTHrP (1–34) or saline for 24 hours and conditioned media harvested (39). $CD11b^+Gr1^+$ cells were isolated from femoral bone marrow and stimulated with osteoblast-derived control- or PTHrP-conditioned media in combination with neutralizing antibodies against VEGF-A and/or IL-6. Consistent with the previous data, PTHrP-conditioned media from osteoblast cultures increased *Mmp9* gene expression (Fig. 6E) and functional MMP-9 (Fig. 6F) in the MDSCs, and these effects were blocked by anti-VEGF-A and/or anti-IL-6 neutralizing antibodies. Furthermore, the effect of PTHrP-conditioned media on MMP-9 expression was suppressed by PP2 (Fig. 6G).

Anti-PTHrP monoclonal antibody treatment decreased MDSC recruitment in PC-3 tumors

Finally, to more rigorously determine the causal relationship between PTHrP and MDSC recruitment, mice bearing $PTHrP^{Hi}$ PC-3 tumors were treated with nonspecific control IgG or anti-human PTHrP monoclonal antibodies. Anti-PTHrP antibodies significantly suppressed tumor growth, but not to the level of $PTHrP^{Lo}$ tumors (Fig. 7A and B). As anti-PTHrP monoclonal antibodies potentially suppress tumor growth via inhibition of autocrine PTHrP effects on tumor cells (Supplementary Fig. S4), tumor tissues were analyzed for MDSC recruitment by immunofluorescence colocalization of $CD11b^+Gr1^+$ cells (Fig. 7C and D). Numbers of $CD11b^+Gr1^+$ cells were decreased in anti-PTHrP antibody-treated or $PTHrP^{Lo}$ tumor tissues, suggesting that reduced PTHrP is causal to decreased MDSCs found in tumor tissues. Serum calcium levels were correlated with PTHrP levels, indicating the functional activity of PTHrP (Fig. 7E). Quantitative RT-PCR analysis in tumor tissues revealed that shRNA-mediated PTHrP knockdown was stable in PC-3 tumor cells during *in vivo* tumor growth, and the correlation between PTHrP and *Mmp9* gene expression (Fig. 7F and G).

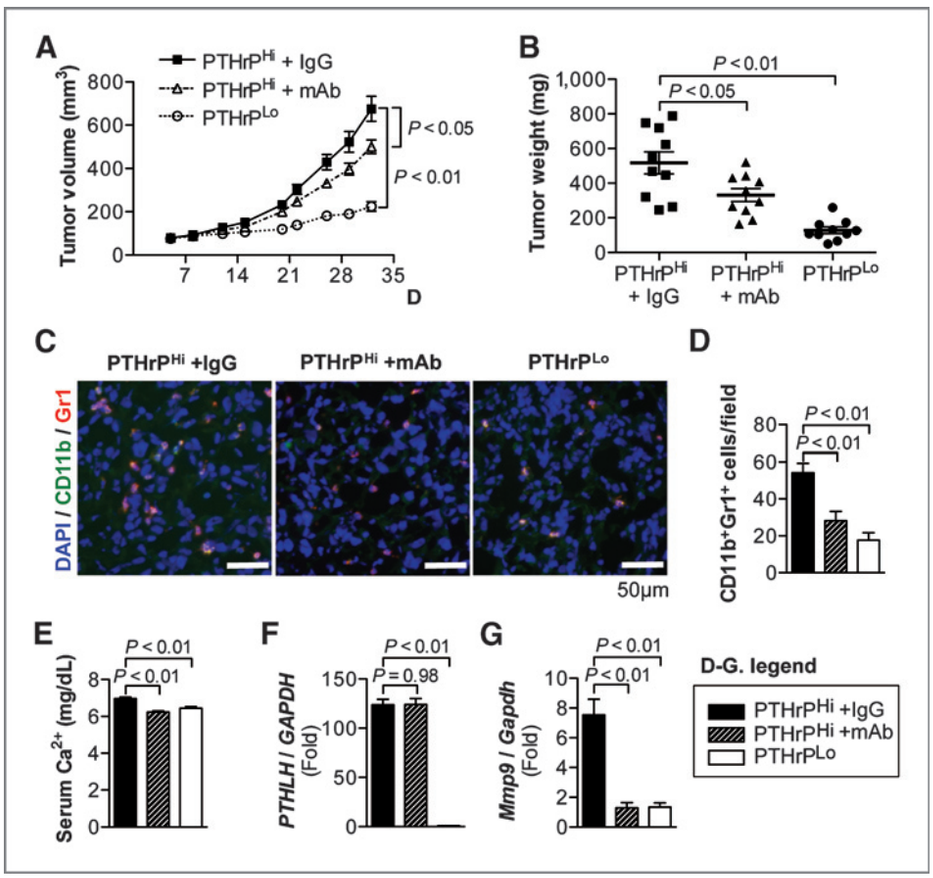

Figure 7. Anti-human PTHrP monoclonal antibody decreased MDSC recruitment in PC-3 tumors. A, tumor growth curve of PC-3 $PTHrP^{Hi}$ tumors treated with control IgG or anti-PTHrP monoclonal antibodies (mAb) and PC-3 $PTHrP^{Lo}$ tumors ($n = 10$ per group). Both *P* values are from linear regression comparison with PC-3 $PTHrP^{Hi}$ IgG tumor group. Data are mean ± SEM. B, individual tumor weight was measured upon necropsy and plotted. Dots, individual measurements (mg). Horizontal lines, mean ± SEM ($n = 10$ per group). C, tumor tissues were sectioned and stained for CD11b (Alexa-Fluor 488), Gr1 (Alexa-Fluor 546), and DAPI. Original magnification, ×40. Scale bars, 50 μm. D, immunofluorescent images were merged and analyzed for $CD11b^+Gr1^+$ cell per microscopic field. Three positively stained nonnecrotic tumor areas were randomly selected for quantification (5 tumors/group). E, sera were collected upon necropsy, followed by calcium assay. F and G, *PTHLH* or *Mmp9* mRNA levels in the pulverized tumor tissue were measured by quantitative RT-PCR ($n = 10$ per group). Data in all bar graphs are mean ± SEM. All *P* values, unless indicated otherwise, are from Student *t* test.

Published OnlineFirst September 26, 2013; DOI: 10.1158/0008-5472.CAN-12-4692

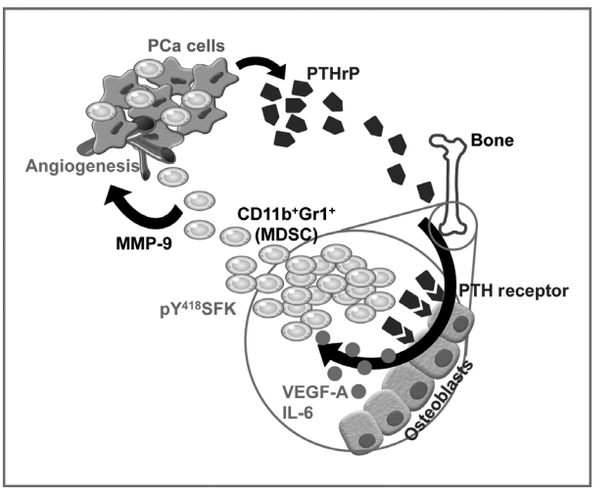

Figure 8. Proposed model of CD11b$^+$Gr1$^+$ cell activation within the bone marrow of prostate tumor hosts via PTHrP. Prostate tumor–derived PTHrP circulates to stimulate VEGF-A and IL-6 expression by osteoblasts, leading to SFK phosphorylation of CD11b$^+$Gr1$^+$ MDSCs. Activation of SFK confers angiogenic potential of MDSCs via increased MMP-9 expression, contributing to prostate cancer growth and angiogenesis.

Discussion

This study provides new evidence that distant tumors stimulate the bone marrow to increase critical component cells in the tumor microenvironment. In brief, prostate cancer–derived PTHrP circulates to potentiate CD11b$^+$Gr1$^+$ cells within the bone marrow via upregulation of IL-6 and VEGF-A in osteoblasts, contributing to tumor growth and angiogenesis (Fig. 8). As a proposed mechanism of CD11b$^+$Gr1$^+$ cell potentiation, these data demonstrate that PTHrP increased activating phosphorylation of SFKs that subsequently increased *Mmp9* gene expression in CD11b$^+$Gr1$^+$ cells, supporting that CD11b$^+$Gr1$^+$ cell-dependent tumor growth is, at least in part, mediated by MMP-9 expression and angiogenesis.

Increasing evidence now clearly supports the critical functions of CD11b$^+$Gr1$^+$ MDSCs in the tumor microenvironment (40). However, the majority of previous studies have been focused either on the roles of MDSCs within the tumor microenvironment (i.e., immune suppression and angiogenesis) or the mechanism of MDSC recruitment to the tumor (41, 42). Given that bone is an essential partner for tumor progression by supplying numerous bone marrow–derived stromal cells, primary tumor cells are speculated to have active mechanisms to interact with the bone/bone marrow (43, 44). The data in this study demonstrate that PTHrP serves as a messenger between the primary tumor and the bone marrow, conferring MDSCs with increased angiogenic potential. PTHrP is a potent bone-modulating cytokine expressed by multiple types of tumor cells such as prostate, breast, lung, and colorectal cancers (45–48). In addition, PTHrP is a key regulator of the "vicious cycle" hypothesis of metastatic tumor–bone interactions (49). However, given that MDSCs are currently considered universally essential components of the tumor microenvironment, not all tumor types express PTHrP, suggesting that PTHrP is not the only factor mediating the interactions between tumor and bone.

The molecular mechanisms of MDSC activation, expansion, and/or mobilization, and ultimately therapeutic approaches targeting the key signaling mechanisms, warrant extensive further investigation. Interestingly, the preliminary studies shown in Supplementary Fig. S5 suggest that PTHrP induces a series of alterations in the bone marrow to mobilize and/or expand MDSCs. Still, questions remain about whether and how PTHrP stimulates differentiation of MDSCs from bone marrow precursors. Nevertheless, this work provides a biological rationale for the clinical application of SFK inhibitors in targeting 2 compartments (i.e., tumor and the microenvironment) simultaneously, of which the mechanism requires further studies. The data in this study demonstrate that activation of SFKs is one of the key signal transduction mechanisms of MDSCs' angiogenic potential, in addition to two other factors, STAT3 and PI3K, that have previously been shown to be implicated in MDSC functions (13, 31). Indeed, SFKs mediate crucial regulatory functions in both tumor cells and stromal cells (e.g., endothelial cells and osteoclasts), suggesting that SFKs are promising therapeutic targets for the suppression of tumor as well as stromal compartments (24, 50).

In conclusion, this study provides evidence that prostate cancers positively regulate the bone marrow microenvironment via PTHrP, IL-6, VEGF-A, and SFKs, thereby increasing the angiogenic potential of CD11b$^+$Gr1$^+$ MDSCs, leading to increased tumor growth.

Disclosure of Potential Conflicts of Interest

No potential conflicts of interest were disclosed.

Authors' Contributions

Conception and design: S.I. Park, L.K. McCauley
Development of methodology: S.I. Park, J. Jones, L.K. McCauley
Acquisition of data (provided animals, acquired and managed patients, provided facilities, etc.): S.I. Park, C. Lee, A.J. Koh, J.W. Seo, F.N. Soki, S.W. Cho
Analysis and interpretation of data (e.g., statistical analysis, biostatistics, computational analysis): S.I. Park, A.J. Koh, S.W. Cho, S. Daignault-Newton, L.K. McCauley
Writing, review, and/or revision of the manuscript: S.I. Park, J. Jones, J.W. Seo, F.N. Soki, S. Daignault-Newton, L.K. McCauley
Administrative, technical, or material support (i.e., reporting or organizing data, constructing databases): S.I. Park, D. Sadler, L.K. McCauley
Study supervision: L.K. McCauley

Acknowledgments

The authors thank Drs. E. Keller, R. Taichman, and K. Pienta for valuable discussion; and Dr. R. Kremer for providing anti-PTHrP monoclonal antibody.

Grant Support

This work was financially supported by the Department of Defense Prostate Cancer Research Program (W81XWH-10-1-0546 and WX81XWH-12-1-0348 to S.I. Park) and the National Cancer Institute Program Project (P01CA093900 to L.K. McCauley). Flow cytometric analyses were supported in part by the National Cancer Institute Cancer Center Support (P30CA068485) to Vanderbilt-Ingram Cancer Center.

The costs of publication of this article were defrayed in part by the payment of page charges. This article must therefore be hereby marked *advertisement* in accordance with 18 U.S.C. Section 1734 solely to indicate this fact.

Received December 28, 2012; revised July 29, 2013; accepted August 12, 2013; published OnlineFirst September 26, 2013.

Published OnlineFirst September 26, 2013; DOI: 10.1158/0008-5472.CAN-12-4692

References

1. Hanahan D, Weinberg RA. Hallmarks of cancer: the next generation. Cell 2011;144:646–74.
2. Shiao SL, Ganesan AP, Rugo HS, Coussens LM. Immune microenvironments in solid tumors: new targets for therapy. Gene Dev 2011;25:2559–72.
3. Park SI, Soki FN, McCauley LK. Roles of bone marrow cells in skeletal metastases: no longer bystanders. Cancer Microenviron 2011;4: 237–46.
4. Park SI, Liao J, Berry JE, Li X, Koh AJ, Michalski ME, et al. Cyclophosphamide creates a receptive microenvironment for prostate cancer skeletal metastasis. Cancer Res 2012;72:2522–32.
5. Yang L, Edwards CM, Mundy GR. Gr-1+CD11b+ myeloid-derived suppressor cells: formidable partners in tumor metastasis. J Bone Miner Res 2010;25:1701–6.
6. Youn J-I, Gabrilovich DI. The biology of myeloid-derived suppressor cells: the blessing and the curse of morphological and functional heterogeneity. Eur J Immunol 2010;40:2969–75.
7. Yang L, DeBusk LM, Fukuda K, Fingleton B, Green-Jarvis B, Shyr Y, et al. Expansion of myeloid immune suppressor Gr+CD11b+ cells in tumor-bearing host directly promotes tumor angiogenesis. Cancer Cell 2004;6:409–21.
8. Zhao F, Obermann S, Wasielewski von R, Haile L, Manns MP, Korangy F, et al. Increase in frequency of myeloid-derived suppressor cells in mice with spontaneous pancreatic carcinoma. Immunology 2009;128: 141–9.
9. Ahn G-O, Brown JM. Influence of bone marrow-derived hematopoietic cells on the tumor response to radiotherapy: experimental models and clinical perspectives. Cell Cycle 2009;8:970–6.
10. Ahn G-O, Tseng D, Liao C-H, Dorie MJ, Czechowicz A, Brown JM. Inhibition of Mac-1 (CD11b/CD18) enhances tumor response to radiation by reducing myeloid cell recruitment. Proc Natl Acad Sci U S A 2010;107:8363–8.
11. Shojaei F, Wu X, Malik AK, Zhong C, Baldwin ME, Schanz S, et al. Tumor refractoriness to anti-VEGF treatment is mediated by CD11b+Gr1+ myeloid cells. Nat Biotechnol 2007;25:911–20.
12. Yang L, Huang J, Ren X, Gorska AE, Chytil A, Aakre M, et al. Abrogation of TGF beta signaling in mammary carcinomas recruits Gr-1+CD11b+ myeloid cells that promote metastasis. Cancer Cell 2008;13:23–35.
13. Schmid MC, Avraamides CJ, Dippold HC, Franco I, Foubert P, Ellies LG, et al. Receptor tyrosine kinases and TLR/IL1Rs unexpectedly activate myeloid cell PI3kγ, a single convergent point promoting tumor inflammation and progression. Cancer Cell 2011;19:715–27.
14. Dayyani F, Gallick GE, Logothetis CJ, Corn PG. Novel therapies for metastatic castrate-resistant prostate cancer. J Natl Cancer Inst 2011; 103:1665–75.
15. Weilbaecher KN, Guise TA, McCauley LK. Cancer to bone: a fatal attraction. Nat Rev Cancer 2011;11:411–25.
16. Li X, Loberg R, Liao J, Ying C, Snyder LA, Pienta KJ, et al. A destructive cascade mediated by CCL2 facilitates prostate cancer growth in bone. Cancer Res 2009;69:1685–92.
17. Liao J, Li X, Koh AJ, Berry JE, Thudi N, Rosol TJ, et al. Tumor expressed PTHrP facilitates prostate cancer-induced osteoblastic lesions. Int J Cancer 2008;123:2267–78.
18. Li J, Karaplis AC, Huang DC, Siegel PM, Camirand A, Yang XF, et al. PTHrP drives breast tumor initiation, progression, and metastasis in mice and is a potential therapy target. J Clin Invest 2011;121:4655–69.
19. Park SI, McCauley LK. Nuclear localization of parathyroid hormone-related peptide confers resistance to anoikis in prostate cancer cells. Endocr Relat Cancer 2012;19:243–54.
20. Park SI, Kim SJ, McCauley LK, Gallick GE. Pre-clinical mouse models of human prostate cancer and their utility in drug discovery. Curr Protoc Pharmacol 2010;Chapter 14:Unit14.15.
21. Jung Y, Shiozawa Y, Wang J, McGregor N, Dai J, Park SI, et al. Prevalence of prostate cancer metastases after intravenous inoculation provides clues into the molecular basis of dormancy in the bone marrow microenvironment. Neoplasia 2012;14:429–39.
22. Tomayko MMM, Reynolds CPC. Determination of subcutaneous tumor size in athymic (nude) mice. Cancer Chemother Pharmacol 1989;24:148–54.
23. Pirih FQ, Michalski MN, Cho SW, Koh AJ, Berry JE, Ghaname E, et al. Parathyroid hormone mediates hematopoietic cell expansion through interleukin-6. PLoS One 2010;5:e13657.
24. Park SI, Zhang J, Phillips KA, Araujo JC, Najjar AM, Volgin AY, et al. Targeting SRC family kinases inhibits growth and lymph node metastases of prostate cancer in an orthotopic nude mouse model. Cancer Res 2008;68:3323–33.
25. Novince CM, Koh AJ, Michalski MN, Marchesan JT, Wang J, Jung Y, et al. Proteoglycan 4, a novel immunomodulatory factor, regulates parathyroid hormone actions on hematopoietic cells. Am J Pathol 2011;179:2431–42.
26. Dougherty KM, Blomme EA, Koh AJ, Henderson JE, Pienta KJ, Rosol TJ, et al. Parathyroid hormone-related protein as a growth regulator of prostate carcinoma. Cancer Res 1999;59:6015–22.
27. Tovar Sepulveda VA, Falzon M. Parathyroid hormone-related protein enhances PC-3 prostate cancer cell growth via both autocrine/paracrine and intracrine pathways. Regul Pept 2002;105: 109–20.
28. Ahn G-O, Brown JM. Matrix metalloproteinase-9 is required for tumor vasculogenesis but not for angiogenesis: role of bone marrow-derived myelomonocytic cells. Cancer Cell 2008;13: 193–205.
29. LeRoy BE, Thudi NK, Nadella MVP, Toribio RE, Tannehill-Gregg SH, van Bokhoven A, et al. New bone formation and osteolysis by a metastatic, highly invasive canine prostate carcinoma xenograft. Prostate 2006;66:1213–22.
30. Abe F, Dafferner AJ, Donkor M, Westphal SN, Scholar EM, Solheim JC, et al. Myeloid-derived suppressor cells in mammary tumor progression in FVB Neu transgenic mice. Cancer Immunol Immunother 2010;59: 47–62.
31. Kujawski M, Kortylewski M, Lee H, Herrmann A, Kay H, Yu H. Stat3 mediates myeloid cell-dependent tumor angiogenesis in mice. J Clin Invest 2008;118:3367–77.
32. Liang W, Kujawski M, Wu J, Lu J, Herrmann A, Loera S, et al. Antitumor activity of targeting SRC kinases in endothelial and myeloid cell compartments of the tumor microenvironment. Clin Cancer Res 2010; 16:924–35.
33. Huang YF, Harrison JR, Lorenzo JA, Kream BE. Parathyroid hormone induces interleukin-6 heterogeneous nuclear and messenger RNA expression in murine calvarial organ cultures. Bone 1998;23: 327–32.
34. Lowik CW, van der Pluijm G, Bloys H, Hoekman K, Bijvoet OL, Aarden LA, et al. Parathyroid hormone (PTH) and PTH-like protein (PLP) stimulate interleukin-6 production by osteogenic cells: a possible role of interleukin-6 in osteoclastogenesis. Biochem Biophys Res Commun 1989;162:1546–52.
35. Esbrit P, Alvarez-Arroyo MV, De Miguel F, Martin O, Martinez ME, Caramelo C. C-terminal parathyroid hormone-related protein increases vascular endothelial growth factor in human osteoblastic cells. J Am Soc Nephrol 2000;11:1085–92.
36. Sabbota AL, Kim H-RC, Zhe X, Fridman R, Bonfil RD, Cher ML. Shedding of RANKL by tumor-associated MT1-MMP activates Src-dependent prostate cancer cell migration. Cancer Res 2010;70: 5558–66.
37. Hallek M, Neumann C, Schaffer M, Danhauser-Riedl S, Bubnoff von N, de Vos G, et al. Signal transduction of interleukin-6 involves tyrosine phosphorylation of multiple cytosolic proteins and activation of Src-family kinases Fyn, Hck, and Lyn in multiple myeloma cell lines. Exp Hematol 1997;25:1367–77.
38. Inngjerdingen M, Torgersen KM, Maghazachi AA. Lck is required for stromal cell-derived factor 1α (CXCL12)-induced lymphoid cell chemotaxis. Blood 2002;99:4318–25.
39. Jin R, Sterling JA, Edwards JR, DeGraff DJ, Lee C, Park SI, et al. Activation of NF-κB signaling promotes growth of prostate cancer cells in bone.Wang QJ, editor. PLoS One 2013;8:e60983.
40. Youn J-I, Kumar V, Collazo M, Nefedova Y, Condamine T, Cheng P, et al. Epigenetic silencing of retinoblastoma gene regulates pathologic differentiation of myeloid cells in cancer. Nat Immunol 2013: 14:211–20.

Published OnlineFirst September 26, 2013; DOI: 10.1158/0008-5472.CAN-12-4692

41. Coffelt SB, Lewis CE, Naldini L, Brown JM, Ferrara N, De Palma M. Elusive identities and overlapping phenotypes of proangiogenic myeloid cells in tumors. Am J Pathol 2010;176:1564–76.
42. Shojaei F, Zhong C, Wu X, Yu L, Ferrara N. Role of myeloid cells in tumor angiogenesis and growth. Trends Cell Biol 2008;18:372–8.
43. Li X, Koh AJ, Wang Z, Soki FN, Park SI, Pienta KJ, et al. Inhibitory effects of megakaryocytic cells in prostate cancer skeletal metastasis. J Bone Miner Res 2011;26:125–34.
44. Li X, Liao J, Park SI, Koh AJ, Sadler WD, Pienta KJ, et al. Drugs which inhibit osteoclast function suppress tumor growth through calcium reduction in bone. Bone 2011;48:1354–61.
45. Kremer R, Li J, Camirand A, Karaplis AC. Parathyroid hormone related protein (PTHrP) in tumor progression. Adv Exp Med Biol 2011;720:145–60.
46. Zhang H, Yu C, Dai J, Keller JM, Hua A, Sottnik JL, et al. Parathyroid hormone-related protein inhibits DKK1 expression through c-Jun-mediated inhibition of β-catenin activationof the DKK1 promoter in prostate cancer. Oncogene 2013 Jun 10.
47. McCauley LK, Martin TJ. Twenty-five years of PTHrP progress: from cancer hormone to multifunctional cytokine. J Bone Miner Res 2012;27:1231–9.
48. Cho SW, Pirih FQ, Koh AJ, Michalski M, Eber MR, Ritchie K, et al. The soluble interleukin-6 receptor is a mediator of hematopoietic and skeletal actions of parathyroid hormone. J Biol Chem 2013;288:6814–25.
49. Guise TA, Yin JJ, Taylor SD, Kumagai Y, Dallas M, Boyce BF, et al. Evidence for a causal role of parathyroid hormone-related protein in the pathogenesis of human breast cancer-mediated osteolysis. J Clin Invest 1996;98:1544–9.
50. Kim MP, Park SI, Kopetz S, Gallick GE. Src family kinases as mediators of endothelial permeability: effects on inflammation and metastasis. Cell Tissue Res 2009;335:249–59.

Appendix 2

Osteal macrophages support physiologic skeletal remodeling and anabolic actions of parathyroid hormone in bone

Sun Wook Cho[a,b], Fabiana N. Soki[a], Amy J. Koh[a], Matthew R. Eber[a], Payam Entezami[a], Serk In Park[a], Nico van Rooijen[c], and Laurie K. McCauley[a,d,1]

[a]Department of Periodontics and Oral Medicine, University of Michigan School of Dentistry, Ann Arbor, MI 48109; [b]Department of Internal Medicine, National Medical Center, Jung-gu, Seoul 100-799, Korea; [c]Department of Molecular Cell Biology, Vrije University Medical Center, 1081 HZ, Amsterdam, The Netherlands; and [d]Department of Pathology, University of Michigan Medical School, Ann Arbor, MI 48109

Edited by John T. Potts, Massachusetts General Hospital, Charlestown, MA, and approved December 10, 2013 (received for review August 21, 2013)

Cellular subpopulations in the bone marrow play distinct and unexplored functions in skeletal homeostasis. This study delineated a unique role of osteal macrophages in bone and parathyroid hormone (PTH)-dependent bone anabolism using murine models of targeted myeloid-lineage cell ablation. Depletion of c-fms$^+$ myeloid lineage cells [via administration of AP20187 in the macrophage Fas-induced apoptosis (MAFIA) mouse model] reduced cortical and trabecular bone mass and attenuated PTH-induced trabecular bone anabolism, supporting the positive function of macrophages in bone homeostasis. Interestingly, using a clodronate liposome model with targeted depletion of mature phagocytic macrophages an opposite effect was found with increased trabecular bone mass and increased PTH-induced anabolism. Apoptotic cells were more numerous in MAFIA versus clodronate-treated mice and flow cytometric analyses of myeloid lineage cells in the bone marrow showed that MAFIA mice had reduced CD68$^+$ cells, whereas clodronate liposome-treated mice had increased CD68$^+$ and CD163$^+$ cells. Clodronate liposomes increased efferocytosis (clearance of apoptotic cells) and gene expression associated with alternatively activated M2 macrophages as well as expression of genes associated with bone formation including *Wnt3a*, *Wnt10b*, and *Tgfb1*. Taken together, depletion of early lineage macrophages resulted in osteopenia with blunted effects of PTH anabolic actions, whereas depletion of differentiated macrophages promoted apoptotic cell clearance and transformed the bone marrow to an osteogenic environment with enhanced PTH anabolism. These data highlight a unique function for osteal macrophages in skeletal homeostasis.

The skeleton provides not only physical support but also housing for numerous subtypes of hematopoietic and immune cells. Several lines of evidence suggest that these skeletal and hematopoietic systems in the bone microenvironment are not only structurally adjacent, but also functionally interactive (1–4). Maintenance of the hematopoietic stem cell niche and B-lymphocyte differentiation has been attributed to osteoblasts (1, 2, 5). T lymphocytes support anabolic actions of parathyroid hormone (PTH) in bone via production of osteoblast stimulating Wnt-10b (6).

Daily intermittent parathyroid hormone (PTH 1–34) administration has prominent anabolic actions in bone and is currently the only approved anabolic agent in the United States for the treatment of osteoporosis. PTH also supports the hematopoietic system by stimulating osteoblastic production of several cytokines, including IL-6 (7, 8), CXCL12 (9), MCP-1 (also known as CCL2) (10, 11), and the soluble IL-6 receptor (sIL6R) (4). PTH improved the success rate of hematopoietic stem cell (HSC) engraftment in hematopoietic malignancies and autoimmune diseases via supporting HSC repopulation of the marrow (12–14). The dependence of hematopoietic lineage cells for PTH anabolic actions is unknown.

Macrophages are mononuclear cells of the myeloid lineage derived from HSCs. Different types of tissue-resident macrophages include Kupffer cells in the liver, Langerhans cells in the lung, and microglia in the brain. In bone, resorbing osteoclasts have been considered the tissue-resident macrophages. However, recent data showed that distinct from osteoclasts bone contains other resident macrophages, especially in the endosteal and periosteal areas (15). These "osteal" macrophages support osteoblast differentiation and mineralization in vitro (15) and play a role in intramembranous bone healing at fracture sites (16). Furthermore, osteal macrophages contribute to the maintenance of the endosteal HSC niches, and loss of osteal macrophages results in the egress of HSCs to the bloodstream (17). Collectively, osteal macrophages play novel roles in both skeletal and hematopoietic systems, yet knowledge of their functional capacities is limited. PTH anabolic actions have been linked to cells of the myeloid lineage via osteoblast derived sIL6R and Stat3 phosphorylation of CD11b$^+$ cells (4). The purpose of this study was to investigate the role of osteal macrophages in bone remodeling and anabolic actions of PTH in bone.

Results

Osteal Macrophages Were Augmented in PTH-Treated Bones. To investigate the role of osteal macrophages in anabolic actions of PTH in bone, changes in myeloid cells with PTH treatment were determined in vivo. Mice (16 wk old, female) were treated with intermittent PTH (50 μg/kg, daily s.c. injection) or saline for 4 wk and immunohistochemical F4/80 staining was performed. F4/80$^+$ osteomacrophages, characterized by spindle-shaped, elongated cytoplasm (15), formed a canopy-like structure over the cuboidal-shaped, bone-lining osteoblasts in endosteal regions of PTH-treated bones (Fig. 1*A*). In periosteal regions, PTH treatment resulted in increased cellularity of relatively cuboidal-shaped bone-lining cells and recruited F4/80$^+$osteal macrophages that

Significance

Cellular subpopulations in the bone marrow play distinct and unexplored functions in the regulation of the skeleton. A type of blood cell that resides in the bone marrow termed "osteal macrophage" was found to play a role in bone homeostasis by supporting bone formation and mediating parathyroid hormone-dependent bone regeneration. Furthermore, induction of cell death in mature macrophages activated the specialized process of efferocytosis (clearance of dead and dying cells), leading to a marrow microenvironment that supported bone formation.

Author contributions: S.W.C. and L.K.M. designed research; S.W.C., F.N.S., A.J.K., M.R.E., P.E., S.I.P., and L.K.M. performed research; N.v.R. and L.K.M. contributed new reagents/analytic tools; S.W.C., M.R.E., P.E., S.I.P., and L.K.M. analyzed data; and S.W.C., A.J.K., S.I.P., and L.K.M. wrote the paper.

The authors declare no conflict of interest.

This article is a PNAS Direct Submission.

[1]To whom correspondence should be addressed. E-mail: mccauley@umich.edu.

This article contains supporting information online at www.pnas.org/lookup/suppl/doi:10.1073/pnas.1315153111/-/DCSupplemental.

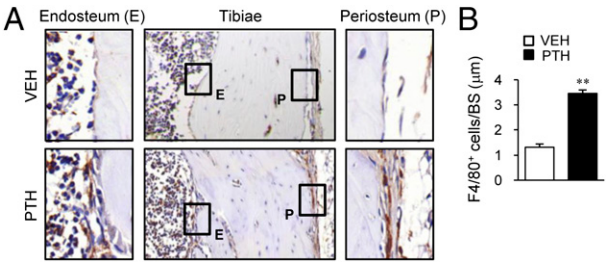

Fig. 1. Osteal macrophages in PTH actions in bone. Mice (16 wk old, female) were treated with intermittent PTH (50 μg/kg) or saline for 4 wk. Tibiae were stained for mouse F4/80. (*A*) Representative images are shown. (*Insets*) Enlarged views of F4/80$^+$ cells (brown stain) in endosteal (E) and periosteal (P) areas. (*B*) Numbers of F4/80$^+$ cells per bone surface in endosteal regions. $n = 6$ per group. $^{**}P < 0.01$ versus vehicle.

covered the periosteal lining cells. In contrast, control bones showed relatively flattened bone-lining cells with few F4/80$^+$ osteal macrophages in endosteal and periosteal areas. Numbers of F4/80$^+$ cells on endosteal bone surfaces were 2.6-fold higher in PTH versus vehicle ($P < 0.01$, Fig. 1*B*). Collectively, osteal macrophages were augmented and in close proximity to PTH-dependent bone remodeling sites, suggesting a role of osteal macrophages in anabolic actions of PTH in bone.

Depletion of Myeloid Cells in MAFIA Mice. The macrophage Fas-induced apoptosis (MAFIA) transgenic mouse model, in which the *Csf1r* (also known as *c-fms*) promoter is engineered to express a *Fas*-based inducible suicide gene and enhanced green fluorescent protein, was used for the depletion of macrophages. With AP20187 ligand injection, systemic and reversible elimination of c-fms$^+$ myeloid lineages was induced (18). After three consecutive days of initial AP20187 (10 mg/kg) injections, 16-wk-old female mice attained greater than 80% depletion of c-fms$^+$ cells as measured via flow cytometric analyses (Fig. S1).

Anabolic Actions of PTH in Macrophage-Depleted MAFIA Mice. Because anabolic effects of PTH in adult murine bone are clearly seen at 6 wk of treatment, the AP20187 ligand injection regimens were optimized for long-term depletion of c-fms$^+$ cells. As shown in Fig. 2*A*, three consecutive injections of AP20187 (10 mg/kg) were followed by booster (1 mg/kg) injections every third day for 3 wk, at which point the dose was reduced to 0.5 mg/kg for the final 3 wk. In preliminary experiments, a higher dose of AP20187 injections in young mice (8–29 d) (five consecutive injections of AP20187 followed by booster injections every other day for 3 wk) resulted in an osteopetrotic phenotype with marked suppression of serum bone turnover markers TRAP5b and P1NP (Fig. S2).

After 6 wk of depletion with the regimen in Fig. 2*A*, the MAFIA mice demonstrated grossly white bones (Fig. 2*B*) with mild anemia (24% decreased percentage of hematocrit). Immunohistochemical F4/80 staining showed a marked reduction of brown-stained macrophages in the bone marrow (Fig. 2*C*), and H&E staining demonstrated extramedullary hematopoiesis in spleen and liver (Fig. S3). Furthermore, flow cytometric analyses showed that mature macrophages displaying the specific GR1$^-$F4/80$^+$c-fms^{int}SSC$^{int/lo}$ markers (19, 20) (Fig. S4) were reduced by 85% (Fig. 2*D*) and CD68$^+$ cells, phagocytosing macrophages (21), by 48% (Fig. 2*E*). Serum bone resorption marker TRAP5b showed a 20% reduction at 2 wk, which was restored at 4 wk in the AP20187 group compared with control (Fig. 2*F*). Serum P1NP, a marker for bone formation, was suppressed 70% at 2 wk and 50% at 4 wk with AP20187 treatment (Fig. 2*G*).

Having confirmed the feasibility of long-term depletion of macrophages in the MAFIA mouse model, 6-wk intermittent PTH (50 μg/kg, daily s.c. injection) was administered after the initial 3 d of AP20187 injections (10 mg/kg) (Fig. 3*A*). After 6 wk, the AP20187 group showed marked reductions of trabecular (55%, Fig. 3*B*) and cortical bone volumes (20%, Fig. 3*C*) via micro computed tomography (μCT) analysis. Furthermore, PTH showed no anabolic effects on either trabecular or cortical bones in the AP20187 group (Fig. 3 *B* and *C*), whereas controls showed significant increases in trabecular (20%, Fig. 3*B*) and cortical bone (7%, Fig. 3*C*) in response to PTH treatment. Histomorphometric analysis showed that PTH-dependent increases in trabecular bone area, thickness, and number and reciprocal decreases of trabecular spaces were attenuated in the AP20187 compared with control group (Fig. 4*A*). These changes were amplified in histomorphometric analysis compared with micro CT analysis, which focused on a narrow region of interest in the metaphyseal area. Osteoclast numbers (OC.N/BS) in tartrate resistant acid phosphate (TRAP)-stained sections (Fig. 4*B*) and serum TRAP5b levels (Fig. 4*C*) were significantly increased with PTH treatment in controls, whereas these PTH effects were lost in the AP20187 group. Furthermore, serum P1NP levels were also increased with PTH in controls, but not in the AP20187 group (Fig. 4*D*), suggesting that PTH induced bone remodeling was attenuated in the macrophage-depleted MAFIA mouse model.

Anabolic Actions of PTH in the Clodronate Liposome Macrophage Depletion Model. The MAFIA mouse model results in a dramatic reduction of all c-fms$^+$ cells. The next approach was focused to deplete mature phagocytic macrophages using clodronate liposomes (22). Intraperitoneal injection of clodronate liposomes (10 μL/g) resulted in 80% depletion of GR1$^-$F4/80$^+$SSC$^{int/lo}$ cells at 24–48 h, with more than 50% of the depleted cells recovered after 72 h (Fig. S5). Hence, clodronate liposomes or PBS liposomes (10 μL/g) were injected for the initial three consecutive days then every third day for 3 wk, and a reduced dose (6 μL/g) was used for the final 3 wk (Fig. 5*A*). After 6 wk of clodronate liposome injections, flow cytometric analyses demonstrated that GR1$^-$F4/80$^+$SSC$^{int/lo}$ macrophages were depleted by 65% (Fig. 5*B*). In notable contrast, CD68$^+$ phagocytic cells were increased

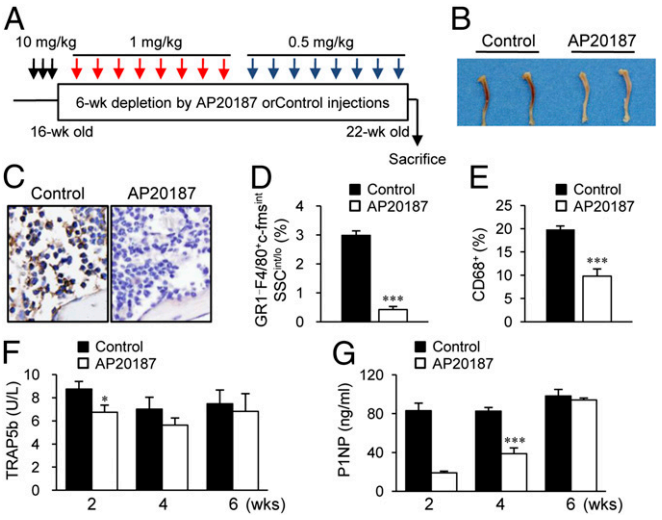

Fig. 2. Long-term depletion of myeloid cells in MAFIA mice. (*A*) Macrophage depletion regimen. MAFIA mice (16 wk old, female) were treated with three consecutive AP20187 (10 mg/kg) injections (black arrows), followed by booster injections every third day (1 mg/kg for 3 wk, then 0.5 mg/kg for 3 wk; red and blue arrows, respectively). (*B*) Photographic representation and (*C*) F4/80$^+$ immunohistochemical staining of tibiae harvested after 6-wk AP20187 or control treatments. Flow cytometric quantification of (*D*) GR1$^-$F4/80$^+$c-fms^{int}SSC$^{int/lo}$ and (*E*) CD68$^+$ cells. Serum samples were collected at 2-, 4-, and 6-wk time points during the 6-wk AP20187 treatment period. (*F*) TRAP5b (units per liter) and (*G*) P1NP (nanograms per milliliter) were measured. Data are mean ± SEM of two independent experiments. $n = 6$–10 per group. $^*P < 0.01$; $^{***}P < 0.001$ versus control.

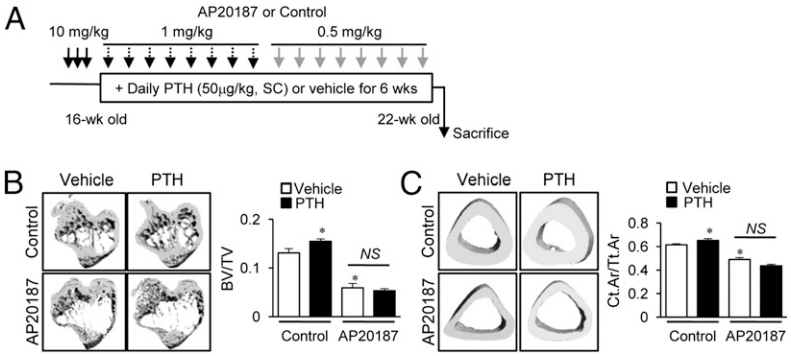

Fig. 3. μCT analyses of bone in long-term depleted MAFIA mice. (*A*) Treatment regimen with PTH and AP20187. MAFIA mice (16 wk old, female) were treated with three consecutive AP20187 (10 mg/kg) injections, followed by booster injections every third day (1 mg/kg for 3 wk, then 0.5 mg/kg for 3 wk). Six weeks of intermittent PTH (50 μg/kg) were started after the initial 3 d. Representative images and quantitative analyses of μCT scanning of tibiae for (*B*) trabecular bone volumes and (*C*) fractional cortical bone areas. All data are means ± SEM of two independent experiments. $n = 8$–10 per group. NS, not significant; $^*P < 0.05$ versus vehicle-treated control.

by 20% (Fig. 5*C*) and $CD11b^+GR1^+F4/80^-$ immature myeloid cells were robustly increased by 60% (Fig. 5*D*).

In contrast to the MAFIA model, long-term depletion of macrophages with clodronate liposomes resulted in high bone mass, independent of PTH (Fig. 5 *E* and *F*). The μCT analyses demonstrated that the trabecular bone volume was significantly increased (20%) in the clodronate versus PBS liposome group (Fig. 5*E*), with no difference noted in cortical bone volume (Fig. 5*F*). Consistently, histomorphometric analysis showed that trabecular bone area and trabecular numbers were significantly increased by 64% and 70%, respectively, and trabecular spacing was reciprocally reduced by 40% in the clodronate versus PBS liposome groups (Fig. 6*A*).

More interestingly, anabolic actions of PTH were even greater in mice administered clodronate versus PBS liposomes. μCT analyses showed PTH-dependent increases of trabecular bone mass were significantly higher in the clodronate versus PBS liposome groups (50% versus 20%, $P < 0.05$, Fig. 5*E*). Furthermore, histomorphometric analyses consistently revealed that PTH enhanced trabecular bone area (96% versus 63%, $P < 0.05$) and trabecular number (57% versus 47%, $P < 0.05$) with clodronate versus PBS liposome treatment (Fig. 6*A*). TRAP staining showed that basal numbers and PTH-dependent increases in osteoclast numbers were similar between the PBS and clodronate liposome groups (Fig. 6*B*).

To further investigate bone remodeling in this model, serum bone turnover markers, including P1NP and TRAP5b, were measured at 4 and 6 wk. As shown in Fig. 6*C*, serum P1NP levels were significantly increased in the clodronate liposome group (30%), and PTH-mediated increases of P1NP were higher in clodronate versus PBS liposome groups with marginal significance (Δ50% versus Δ81%, $P = 0.07$) at 4 wk (Fig. 6*C*). However, basal serum TRAP5b levels and PTH-dependent increases were similar between clodronate and PBS liposome groups at both 4 and 6 wk (Fig. 6*D*). Collectively, clodronate treatment resulted in higher bone mass and amplified PTH anabolism with paralleled increases in serum P1NP, suggesting that these bone changes resulted from enhanced bone formation rather than inhibition of bone resorption.

Clodronate-Targeted Macrophages Stimulated the Mononuclear Phagocytic System. In contrast to the MAFIA mouse model, depletion of macrophages by clodronate liposomes resulted in high bone mass with enhanced PTH anabolic actions. A key difference between the MAFIA and clodronate liposome mouse models was the change in $CD68^+$ cells. Although $GR1^-F4/80^+SSC^{int/lo}$ macrophages were reduced in both MAFIA and clodronate liposome models, the percentages of $CD68^+$ cells were oppositional. $CD68^+$ cells were decreased in the MAFIA mouse model (Fig. 2*E*) and increased in the clodronate mouse model (Fig. 5*C*). Because CD68 has been referred to as an antigen-presenting phagocyte (19, 20), we evaluated the bone marrow microenvironmental changes in the clodronate liposome mouse model.

TUNEL staining of bone sections after 6 wk of treatment revealed that the increase of $TUNEL^+$ apoptotic cells in clodronate liposome-treated mice was much less than that in the MAFIA mouse model (fourfold versus 18-fold, $P < 0.01$, Fig. 7 *A* and *B*). Because both clodronate liposomes and MAFIA/AP20187 injections resulted in similar macrophage depletions at 6 wk, 85% (Fig. 2*D*) and 75% (Fig. 5*B*), respectively, we deduced that cell clearing processes were activated in the clodronate liposome mouse model, which resulted in the notable differences of $TUNEL^+$ cells between MAFIA and clodronate liposome mice. Indeed, flow cytometric analyses showed that cells stained

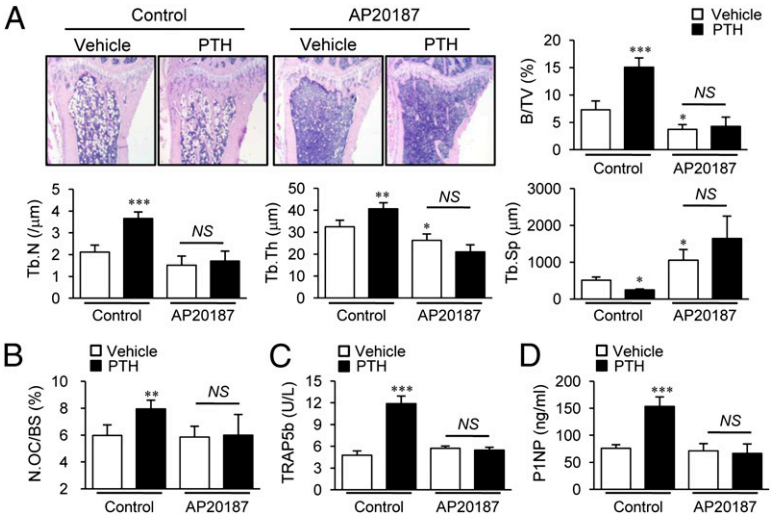

Fig. 4. Bone histomorphometric and serum analyses in long-term depleted MAFIA mice. Histomorphometric analyses of tibiae using the experimental design in Fig. 3*A*. (*A*) Histologic images and static morphometric parameters, including bone volume (BV/TV), trabecular number (Tb.N), trabecular thickness (Tb.Th), and trabecular spacing (Tb.Sp). (*B*) $TRAP^+$ osteoclast numbers (N.OC/BS) were determined. Serum (*C*) TRAP5b (units per liter) and (*D*) P1NP (nanograms per milliliter) levels determined at 6 wk. Data are mean SEM of two independent experiments. $n = 8$–10 per group. NS, not significant; $^*P < 0.05$; $^{**}P < 0.01$; $^{***}P < 0.001$ versus vehicle-treated control (the leftmost column of each graph).

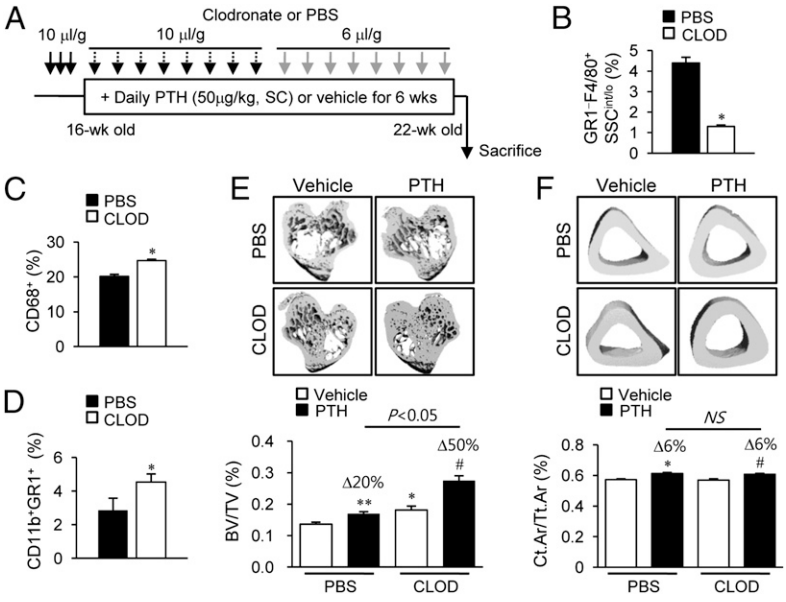

Fig. 5. Bone marrow FACs and μCT analyses in clodronate liposome-treated mice. (*A*) Treatment regimen with clodronate liposomes and PTH. Mice (16 wk old, female) were treated with three consecutive injections of clodronate liposomes (10 μL/g), followed by booster injections every third day (10 μL/g for 3 wk, then 6 μL/g for 3 wk). Six weeks of intermittent PTH (50 μg/kg) were started 3 d after the initiation of clodronate treatment. (*B–D*) Flow cytometric analyses of the whole bone marrow cells. Quantitative analyses of (*B*) $GR1^{-}F4/80^{+}SSC^{int/lo}$ cells, (*C*) $CD68^{+}$ cells, and (*D*) $CD11b^{+}GR1^{+}$ cells. Representative images and graphs (below) of μCT analyses of (*E*) trabecular bone volumes and (*F*) fractional cortical bone areas. Data are mean ± SEM of two independent experiments. n = 10–15 per group. CLOD, clodronate liposome; NS, not significant; PBS, PBS liposome. $^{*}P < 0.05$; $^{**}P < 0.01$ versus vehicle-treated PBS; $^{\#}P < 0.05$ versus vehicle-treated CLOD.

with the $CD163^{+}$ antibody, a member of the scavenger receptor cysteine-rich superfamily (23), were significantly increased with clodronate liposome treatment (Fig. 7*C*).

Bone microenvironments were further investigated. Bone marrow gene expression was investigated after 4 wk of treatment with clodronate liposomes. Real-time PCR analyses showed that genes related to efferocytosis and the M2 phenotype, including *MER receptor kinase*, *milk fat globule-EGF factor 8* (*MFG-E8*), *mannose receptor* (*MRC1*), *macrophage scarvenger receptor 1* (*MSR 1*), *scavenger receptors* (*SR-A* and *CD36*), *IL-10*, and *arginase I*, were up-regulated with clodronate treatment, whereas inflammation-related genes such as *IL-12*, *TNFα*, *IL-1β*, and *iNOS* were not changed between groups (Fig. 7*D*). Protein levels of TGF-β1 were increased with clodronate treatment versus PBS (Fig. 7*E*). Moreover, mRNA expressions of several osteotropic factors known to support PTH anabolic actions were up-regulated in 4-wk-clodronate liposome-treated bone marrow. *TGF-β1* (Fig. 7*F*), *Wnt-3a* (Fig. 7*G*), and *Wnt-10b* (Fig. 7*H*) were up-regulated with clodronate liposome treatment. The PTH-dependent increases in *TGF-β1* (Fig. 7*F*) and *Wnt-3a* (Fig. 7*G*) were higher in clodronate- than in PBS liposome-treated marrows, whereas Wnt-10b was significantly increased by PTH only in the clodronate liposome group (Fig. 7*H*). Collectively, clodronate liposome treatment resulted in increased M2 macrophages as well as increased tissue regenerating factors.

Discussion

The functional role of osteal macrophages was initially established in supporting the maintenance of HSC niches and stimulating intramembranous bone formation in fracture sites (15–17). The actions of macrophages in normal bone remodeling are as yet unclear. The present study showed that osteal macrophages supported bone remodeling in the adult murine skeletal system and that macrophage depletion inhibited PTH anabolic actions in bone. The intriguing finding in this study was that clodronate liposome-induced apoptosis of macrophages paradoxically activated the mononuclear phagocyte system and changed the bone marrow into an osteogenic microenvironment inducing bone formation and augmentation of PTH anabolic actions.

Previous data demonstrated that osteal macrophages stimulated differentiation and mineralization of osteoblasts in vitro,

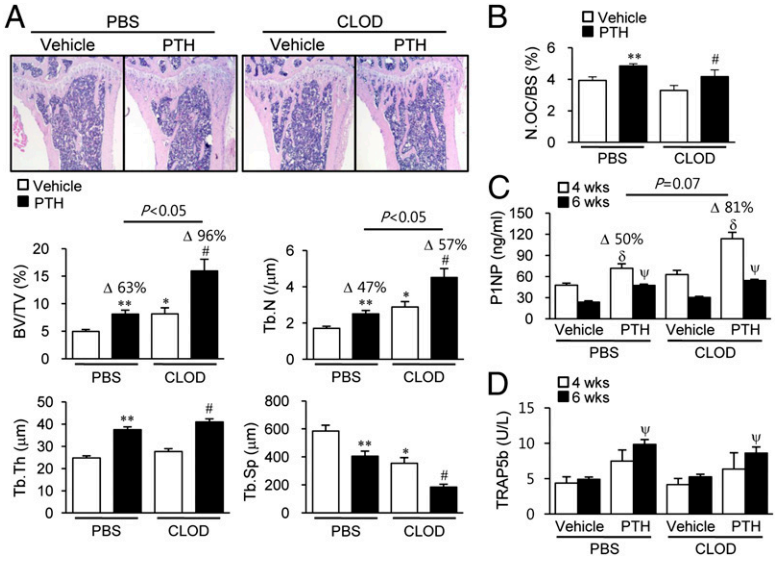

Fig. 6. Bone histomorphometric and serum analyses in clodronate liposome-treated mice. Histomorphometric analyses of tibiae using the experimental design in Fig. 5*A*. (*A*) Representative images with histomorphometric analyses. (*B*) Osteoclast numbers per bone volume (N.OC/BS) measured in TRAP-stained sections. $^{*}P < 0.05$; $^{**}P < 0.01$ versus vehicle-treated PBS. (*C* and *D*) Serum (*C*) P1NP (nanograms per milliliter) and (*D*) TRAP5b (units per liter) measured at 4 and 6 wk. $^{\#}P < 0.05$ versus vehicle-treated CLOD; $^{\delta}P < 0.05$ versus vehicle in each group at 4 wk; $^{\Psi}P < 0.05$ versus vehicle in each group at 6 wk. Data are mean ± SEM of two independent experiments. n = 10–15 per group. CLOD, clodronate liposome; PBS, PBS liposome.

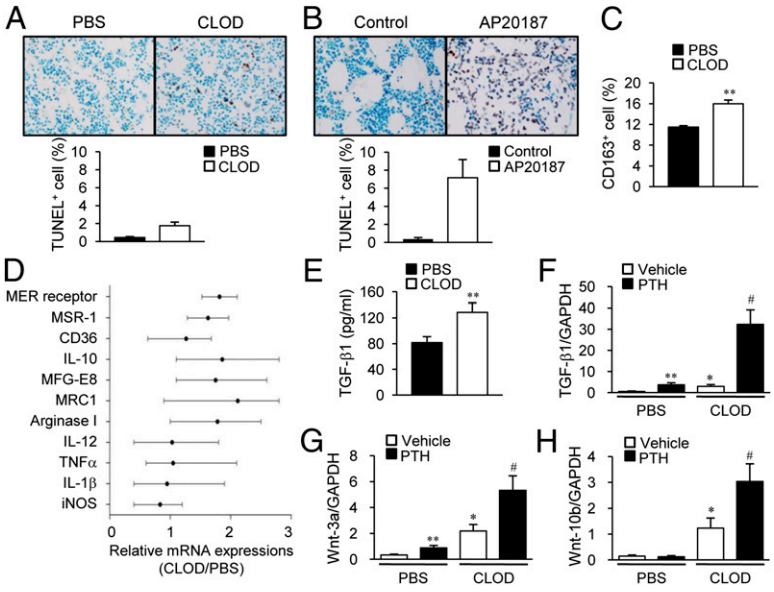

Fig. 7. Bone microenvironment changes in macrophage-depleted mice. (*A*) TUNEL staining on tibial sections in mice (16 wk old, female) treated with clodronate liposomes following the regimen in Fig 5*A*. (*B*) TUNEL staining on tibial sections in mice (16 wk old, female) treated with the regimen in Fig 2*A*. TUNEL$^+$ cells were enumerated. $n = 7$ per group. (*C–E*) Mice (16 wk old, female) were treated with clodronate liposomes; three consecutive injections were followed by booster injections (every third day, 10 μL/g for 3 wk and 6 μL/g for 1 wk). (*C*) Flow cytometric analysis of whole marrow cells using anti-CD163 antibody. (*D*) Genes related to M1/M2 macrophage were analyzed by real-time PCR from whole marrow mRNA. (*E*) Protein levels of TGF-β1 in bone marrow. $^{**}P < 0.01$ versus vehicle. (*F–H*) Mice (16 wk old, female) were treated with clodronate liposomes; three consecutive injections were followed by booster injections (every third day, 10 μL/g for 3 wk and 6 μL/g for 1 wk). Four weeks of intermittent PTH (50 μg/kg) were started after the initial 3 d. Whole marrow mRNA was analyzed by real-time PCR using specific primers for (*F*) *Tgfb1*, (*G*) *Wnt3a*, and (*H*) *Wnt10b*. $^{*}P < 0.05$; $^{**}P < 0.01$ versus vehicle-treated PBS; $^{\#}P < 0.05$ versus vehicle-treated CLOD. Data are mean ± SEM of two independent experiments. $n = 6$ per group. CLOD, clodronate liposome; PBS, PBS liposome.

and depletion of osteal macrophages resulted in loss of mature osteoblasts in bone remodeling sites in vivo (15). The present study further demonstrated that osteal macrophages support bone formation using the MAFIA mouse model. After the 6-wk AP20187 regime, and using the stringent criteria put forth by Chow et al. (21), more than 80% of macrophages were depleted. In contrast, osteoclasts were not significantly affected, likely owing to the staggered administration of the AP20187 after the initial dosing. This suggests that osteoclastogenesis is more robust and/or a preferred pathway of myeloid lineage differentiation in bone.

Both trabecular and cortical bone volumes were significantly decreased with AP20187-induced macrophage depletion. Serum P1NP levels were significantly decreased at 2 (70%) and 4 (50%) wk whereas TRAP5b showed mild suppression in the AP20187-treated group, suggesting that low bone mass in MAFIA depleted mice mainly resulted from the diminution of bone formation. Furthermore, depletion of macrophages with AP20187 treatment completely blocked PTH anabolic actions in bone with inhibition of PTH-dependent increases of the serum bone turnover markers P1NP and TRAP5b. This reinforces the notion that osteal macrophages play a pivotal role in bone anabolism.

To investigate the effects of osteal macrophages on normal bone remodeling and PTH anabolic actions in bone, long-term depletion of macrophages was essential. Because of the critical role of macrophages in general health, it was not feasible to obtain total macrophage depletion without dire consequences. In the present study, several different regimens were tested and the current one was selected with less than 10% mortality and morbidity (infection etc.). Although the depletion percentages of c-fms$^+$ cells were moderate (50%) at 6 wk, further macrophage-specific analyses via flow cytometry, using F4/80 and GR1, showed greater than 80% macrophage depletion via the current regimen and noted alteration in bone phenotypes. The use of the MAFIA mouse in bone biology could seem problematic because osteoclasts might be affected. Indeed, when we used higher or more frequent doses of AP20187 we experienced moderate to severe suppression of osteoclasts with osteopetrotic phenotypes. The mild depletion regimen used in the current study allowed for long-term macrophage-specific reductions to a level that revealed inhibition of bone accrual in normal bone remodeling and PTH anabolic processes.

This study revealed an intriguing finding, that the treatment with clodronate liposomes in vivo paradoxically showed evidence of stimulating the mononuclear phagocyte system for cell clearance, a process termed efferocytosis, and changed the bone microenvironment into one conducive for bone mass accrual and increased PTH anabolic sensitivity. The clodronate liposome model was introduced to further validate the role of osteal macrophages in bone anabolism by using a second and more narrowly focused macrophage depletion model mechanistically unrelated to the MAFIA mouse model. Similar to the MAFIA mouse model, the depletion regimen was adjusted to achieve moderate macrophage depletions with minimum mortality and morbidity. As a result, macrophages reached 65% depletion yet with marked compensatory increases of immature myeloid precursor cells (CD11b$^+$GR1$^+$ cells). One of the notable differences between these two models was that phagocytic myeloid CD68$^+$ cells were reduced in MAFIA mice but increased in clodronate liposome-treated mice. CD68 has been established as a marker for phagocytic myeloid cells including macrophages, dendritic cells, or neutrophils, rather than a specific marker for macrophages (19). These opposite directional changes of CD68$^+$ cell percentages allowed us to hypothesize that selective depletion of macrophages undergoing engulfment with the clodronate liposome treatment led to compensatory increases in myeloid precursor cells and expansion of the activating mononuclear phagocytic system to clear apoptotic cells and debris.

The process of removing dead cell bodies, efferocytosis, is a rapid host defense process for maintaining tissue homeostasis (24). During efferocytosis, apoptotic cells release "find me" and "eat me" signals and are recognized by macrophages or other phagocytic cells. Consistent with CD68$^+$ cells, CD163$^+$ cells (23), another marker for phagocytosis, were also increased in clodronate liposome-treated mice. Furthermore, analysis of gene expression showed that the MFG-E8/MER receptor axis, and the scavenger receptors [CD36 and class A macrophage scavenger receptor (SR-A)] were up-regulated in the clodronate liposome-treated group compared with controls, supporting this hypothesis. This compensatory mechanism was not possible in MAFIA mice, because the AP20187 depletion affected a broad range of c-fms$^+$ myeloid cells, from early precursors to mature macrophages.

More interestingly, M2-macrophage–related genes (IL-10 and arginase I) were increased with reciprocal down-regulation of M1-macrophage–related genes (IL-1, IL-12, iNOS, and TNFα) in the clodronate liposome-treated mice compared with the controls. Macrophages polarize into two different phenotypes (25, 26): M1 macrophages are classically activated by IFNγ or bacterial LPS and have proinflammatory functions, such as regulating antigen presentation to T cells. In contrast, M2 macrophages are alternatively activated by IL-8 or M-CSF and participate in cell clearance or wound healing processes with anti-inflammatory

functions. Recent studies showed that several human pathologic conditions with impaired efferocytosis tend to activate M2 macrophage polarization in an attempt to overcome those pathologic conditions (27–29). This study showed that long-term stimulation of macrophage apoptosis and partial depletion of mature macrophages resulted in not only activation of efferocytosis but also in stimulation of macrophage polarization. In addition, these microenvironmental changes were accompanied by an increase of several osteogenic factors such as canonical Wnts and TGF-β1. Wnt-3a and Wnt-10b represent canonical Wnt family members with well-established strong anabolic signaling in bone. Interestingly, recent studies demonstrated that macrophage-derived Wnt proteins are essential for tissue regeneration in kidney (30, 31) and liver (32). In particular, phagocytosis of apoptotic debris was found to stimulate macrophage production of Wnt-3a, which mediated hepatocyte regeneration (32). Corroborating these previous studies, activated phagocytosis in the present study up-regulated Wnt-3a and Wnt-10b in the bone microenvironment, which provided favorable conditions for bone formation, suggesting that the biologic process of cell clearance is commonly followed by signaling for tissue regeneration.

TGF-β1 is a crucial factor produced during efferocytosis (33, 34) and alternative macrophage polarization (35). It is also released and activated by bone-resorbing osteoclasts and recruits mesenchymal progenitor cells to bone remodeling sites, supporting bone formation (36). In an irradiation-induced bone marrow ablation model, PTH was found to increase bone more robustly in association with increased macrophages and TGF-β1 (13). The up-regulation of TGF-β1 in the present study also links to enhanced bone formation ability and PTH anabolic actions.

Maintaining bone homeostasis is an elaborate process based on cellular interactions between osteoclasts, osteocytes, and osteoblasts, and the coupling of bone resorption to bone formation. The present study demonstrated that osteal macrophages play a role in bone remodeling as another cellular component via supporting bone formation and mediating PTH-dependent anabolic actions in bone. Furthermore, induced efferocytosis, linked to M2 macrophage polarization, transformed the bone microenvironment into an osteogenic one via up-regulating canonical Wnts and TGF-β1 production in bone. In conclusion, osteal macrophages in the bone marrow microenvironment highly and favorably affect bone metabolism in support of regeneration and formation.

Materials and Methods

Two murine models of macrophage depletion included the genetic MAFIA model and a clodronate liposome administered model. After 6 wk of intermittent PTH treatment, bone phenotypes were analyzed histomorphometrically, and via microCT analysis. The bone marrow microenvironment was characterized by standard flow cytometric analyses, immunohistochemical staining, real-time PCR, and biochemical assays. More details are included in *SI Materials and Methods*.

ACKNOWLEDGMENTS. This work was supported in part by the National Institutes of Health Grants DK053904 and CA093900 (to L.K.M.), Department of Defense Grant W81XWH-12-1-0348 (to S.I.P.), and National Medical Center, Research Institute (Seoul, Korea) Grant NMC2013-MS-02 (to S.W.C.).

1. Wu JY, et al. (2008) Osteoblastic regulation of B lymphopoiesis is mediated by Gsalpha-dependent signaling pathways. *Proc Natl Acad Sci USA* 105(44):16976–16981.
2. Calvi LM, et al. (2003) Osteoblastic cells regulate the haematopoietic stem cell niche. *Nature* 425(6960):841–846.
3. Weber JM, et al. (2006) Parathyroid hormone stimulates expression of the Notch ligand Jagged1 in osteoblastic cells. *Bone* 39(3):485–493.
4. Cho SW, et al. (2013) The soluble interleukin-6 receptor is a mediator of hematopoietic and skeletal actions of parathyroid hormone. *J Biol Chem* 288(10):6814–6825.
5. Zhu J, et al. (2007) Osteoblasts support B-lymphocyte commitment and differentiation from hematopoietic stem cells. *Blood* 109(9):3706–3712.
6. Terauchi M, et al. (2009) T lymphocytes amplify the anabolic activity of parathyroid hormone through Wnt10b signaling. *Cell Metab* 10(3):229–240.
7. Li X, Qin L, Partridge NC (2008) *In vivo* parathyroid hormone treatments and RNA isolation and analysis. *Methods Mol Biol* 455:79–87.
8. Onyia JE, Bidwell J, Herring J, Hulman J, Hock JM (1995) *In vivo*, human parathyroid hormone fragment (hPTH 1-34) transiently stimulates immediate early response gene expression, but not proliferation, in trabecular bone cells of young rats. *Bone* 17(5): 479–484.
9. Jung Y, et al. (2006) Regulation of SDF-1 (CXCL12) production by osteoblasts; a possible mechanism for stem cell homing. *Bone* 38(4):497–508.
10. Li X, et al. (2007) Determination of dual effects of parathyroid hormone on skeletal gene expression *in vivo* by microarray and network analysis. *J Biol Chem* 282(45):33086–33097.
11. Li X, et al. (2007) Parathyroid hormone stimulates osteoblastic expression of MCP-1 to recruit and increase the fusion of pre/osteoclasts. *J Biol Chem* 282(45):33098–33106.
12. Adams GB, et al. (2007) Therapeutic targeting of a stem cell niche. *Nat Biotechnol* 25(2):238–243.
13. Koh AJ, et al. (2011) An irradiation-altered bone marrow microenvironment impacts anabolic actions of PTH. *Endocrinology* 152(12):4525–4536.
14. Pirih FQ, et al. (2010) Parathyroid hormone mediates hematopoietic cell expansion through interleukin-6. *PLoS ONE* 5(10):e13657.
15. Chang MK, et al. (2008) Osteal tissue macrophages are intercalated throughout human and mouse bone lining tissues and regulate osteoblast function *in vitro* and *in vivo*. *J Immunol* 181(2):1232–1244.
16. Alexander KA, et al. (2011) Osteal macrophages promote *in vivo* intramembranous bone healing in a mouse tibial injury model. *J Bone Miner Res* 26(7):1517–1532.
17. Winkler IG, et al. (2010) Bone marrow macrophages maintain hematopoietic stem cell (HSC) niches and their depletion mobilizes HSCs. *Blood* 116(23):4815–4828.
18. Burnett SH, et al. (2004) Conditional macrophage ablation in transgenic mice expressing a Fas-based suicide gene. *J Leukoc Biol* 75(4):612–623.
19. Kunisch E, et al. (2004) Macrophage specificity of three anti-CD68 monoclonal antibodies (KP1, EBM11, and PGM1) widely used for immunohistochemistry and flow cytometry. *Ann Rheum Dis* 63(7):774–784.
20. Andreeva ER, Pugach IM, Orekhov AN (1997) Subendothelial smooth muscle cells of human aorta express macrophage antigen in situ and *in vitro*. *Atherosclerosis* 135(1): 19–27.
21. Chow A, et al. (2011) Bone marrow CD169+ macrophages promote the retention of hematopoietic stem and progenitor cells in the mesenchymal stem cell niche. *J Exp Med* 208(2):261–271.
22. Van Rooijen N, Sanders A (1994) Liposome mediated depletion of macrophages: mechanism of action, preparation of liposomes and applications. *J Immunol Methods* 174(1-2):83–93.
23. Lau SK, Chu PG, Weiss LM (2004) CD163: A specific marker of macrophages in paraffin-embedded tissue samples. *Am J Clin Pathol* 122(5):794–801.
24. Bratton DL, Henson PM (2011) Neutrophil clearance: When the party is over, clean-up begins. *Trends Immunol* 32(8):350–357.
25. Lawrence T, Natoli G (2011) Transcriptional regulation of macrophage polarization: Enabling diversity with identity. *Nat Rev Immunol* 11(11):750–761.
26. Mantovani A, Sozzani S, Locati M, Allavena P, Sica A (2002) Macrophage polarization: Tumor-associated macrophages as a paradigm for polarized M2 mononuclear phagocytes. *Trends Immunol* 23(11):549–555.
27. Hodge S, et al. (2011) Cigarette smoke-induced changes to alveolar macrophage phenotype and function are improved by treatment with procysteine. *Am J Respir Cell Mol Biol* 44(5):673–681.
28. Mares CA, et al. (2011) Defect in efferocytosis leads to alternative activation of macrophages in Francisella infections. *Immunol Cell Biol* 89(2):167–172.
29. Yamamoto S, et al. (2011) Macrophage polarization by angiotensin II-type 1 receptor aggravates renal injury-acceleration of atherosclerosis. *Arterioscler Thromb Vasc Biol* 31(12):2856–2864.
30. Lin SL, et al. (2010) Macrophage Wnt7b is critical for kidney repair and regeneration. *Proc Natl Acad Sci USA* 107(9):4194–4199.
31. Reddy SM, et al. (2002) Phagocytosis of apoptotic cells by macrophages induces novel signaling events leading to cytokine-independent survival and inhibition of proliferation: Activation of Akt and inhibition of extracellular signal-regulated kinases 1 and 2. *J Immunol* 169(2):702–713.
32. Boulter L, et al. (2012) Macrophage-derived Wnt opposes Notch signaling to specify hepatic progenitor cell fate in chronic liver disease. *Nat Med* 18(4):572–579.
33. Zarin AA, Behmanesh M, Tavallaei M, Shohrati M, Ghanei M (2010) Overexpression of transforming growth factor (TGF)-beta1 and TGF-beta3 genes in lung of toxic-inhaled patients. *Exp Lung Res* 36(5):284–291.
34. Medeiros AI, Serezani CH, Lee SP, Peters-Golden M (2009) Efferocytosis impairs pulmonary macrophage and lung antibacterial function via PGE2/EP2 signaling. *J Exp Med* 206(1):61–68.
35. Gong D, et al. (2012) TGFβ signaling plays a critical role in promoting alternative macrophage activation. *BMC Immunol* 13:31.
36. Tang Y, et al. (2009) TGF-beta1-induced migration of bone mesenchymal stem cells couples bone resorption with formation. *Nat Med* 15(7):757–765.